Journal of Power Sources 263 (2014) 315–331

Contents lists available at ScienceDirect

Journal of Power Sources

journal homepage: www.elsevier.com/locate/jpowsour

Review

Review and analysis of characterization methods and ionic conductivities for low-temperature solid oxide fuel cells (LT-SOFC)

Janne Patakangas*, Ying Ma, Yifu Jing, Peter Lund

Department of Applied Physics, Aalto University, FI-00076 Aalto, Finland

HIGHLIGHTS

- Conductivities of doped ceria/carbonate composite electrolytes have been reviewed.
- Special attention has been paid on the measurement methods.
- Impedance, constant current and product analysis methods are presented and compared.
- The results from the methods cannot be directly compared with each other.
- Recommendations on conductivity measurements of composite electrolytes are given.

ARTICLE INFO

Article history:
Received 19 August 2013
Received in revised form
7 March 2014
Accepted 3 April 2014
Available online 8 May 2014

Keywords:
LT-SOFC
Ionic conductivity
Doped ceria/carbonate electrolyte
Electrochemical impedance spectroscopy
Constant current measurement
Product analysis

ABSTRACT

In recent years, doped ceria/carbonate composite is one of the most researched low-temperature SOFC electrolyte. Its ionic conductivity, which strongly influences the performance of the fuel cell, can be measured with several different methods including EIS, constant current and product analysis measurements. The conductivities of similar materials measured under similar conditions seem to vary quite much, which could be partly explained by the sample preparation affecting the properties of the electrolyte. However, we found that the used measurement approach may impose even a larger uncertainty. Therefore, results from different conductivity measurement techniques may not be comparable. In this article, conductivities of doped ceria/carbonate composites and measurement techniques employed in recent articles have been reviewed. Pros and cons of the different measurement methods are analyzed and discrepancies found in the measured conductivity values are explained. Finally, recommendations on conductivity measurements of LT-SOFC composite electrolytes are given.

1. Introduction

A fuel cell is a promising energy conversion technology that directly converts chemical energy of fuel to electricity. Among different types of fuel cells available, a solid oxide fuel cell (SOFC) has shown great potential for commercial scale production. A traditional SOFC needs to be operated at high temperature (800 °C–1000 °C) to reach adequate ionic conductivity in the YSZ (yttria stabilized zirconia) electrolyte [1]. Other advantages from a higher operating temperature, besides the increased conductivity, include faster electrode reactions excluding the need of expensive catalysts, fuel flexibility due to internal reforming, cogeneration possibility due to the high temperature of the waste heat from the fuel cell, etc. [2]. However, several disadvantages can also be identified such as mechanical and chemical incompatibilities as well as stability issues of the materials used, long start-up times and high cost of the balance-of-plant (BOP) parts [2]. Therefore, research on thin electrolytes and/or new electrolyte materials suitable for lower operating temperatures (300 °C–800 °C) is highly motivated. Samarium and gadolinium doped ceria (SDC and GDC respectively; ceria = cerium oxide) are promising materials for low-temperature solid oxide fuel cells (LT-SOFC) as they show a higher ionic conductivity than YSZ. For example, the oxygen ion conductivity of SDC is around 0.1 S cm^{-1} at 800 °C while YSZ reaches the same value at around 1000 °C [1]. Unfortunately, doped ceria may suffer from mixed electron/ion conductivity which leads to reduced fuel cell performance. In the recent decade it has been widely reported that the addition of salts or hydrates as a second phase into doped ceria can significantly improve the ionic conductivity of the electrolyte due to a composite effect. Among the various composite materials, the addition of carbonate has shown

* Corresponding author. Tel.: +358 505122634.
E-mail addresses: janne.patakangas@aalto.fi (J. Patakangas), ying.ma@aalto.fi (Y. Ma), yifu.jing@aalto.fi (Y. Jing), peter.lund@aalto.fi (P. Lund).

http://dx.doi.org/10.1016/j.jpowsour.2014.04.008
0378-7753/

high potential. For example, a fuel cell with a SDC/$LiNaCO_3$ composite electrolyte has reached a power density of 1700 mW cm^{-2} at 650 °C when H_2, air and CO_2 gases were used [3].

A fuel cell is comprised of two (porous) electrodes and a (dense) electrolyte. The reactions occur on the electrodes while the ions are transported through the electrolyte. The ionic conductivity is thus an important property of the electrolyte (and the fuel cell) characterizing its performance. There are several review papers on doped ceria and doped ceria/carbonate composite electrolytes, but their emphasis is more on the materials, including synthesis, conduction mechanisms and applications [4–8]. However, even though several different measurement methods have been used for determining the ionic conductivity of the electrolytes, there has been no comparison between the methods used for the LT-SOFC materials. Each of the methods have their advantages and disadvantages, which makes a straightforward comparison of results and evaluation of the properties of the electrolytes difficult. Therefore, in this article we provide a profound overview of the conductivities of recent doped ceria/carbonate composites used in ceramic fuel cells, with a particular emphasis on different measurement methods. In the first section, we give a short introduction of the doped ceria/carbonate composite electrolyte materials, after which general information about the measurement methods are elaborated. Then an overview of the methods and the results acquired by each method are given for impedance, constant current and product analysis measurements. Finally, conclusions for the methods are drawn and recommendations about future measurements are given.

2. Doped ceria/carbonate composites

Ceria crystallizes into a fluorite structure between the room temperature and the melting point [9]. Even though the fluorite structure is quite open, the (oxygen) ion conductivity of pure ceria is relatively low. To enhance the conductivity, some of the Ce^{4+} cations have to be substituted with aliovalent cations to increase the number of oxygen vacancies. The highest conductivities of singly doped cerias have been achieved when the ionic radius of the cations is close to that of Ce^{4+} and the charge of the cation is 3+, i.e. with samarium and gadolinium doped cerias [1]. $Sm_xCe_{1-x}O_{2-\delta}$ and $Gd_xCe_{1-x}O_{2-\delta}$ have the highest reported conductivities with x ranging between 0.1 and 0.2 [1,10]. As mentioned earlier, mixing carbonates with doped ceria enhances the properties of the electrolyte. Among different carbonate compounds, lithium, sodium and potassium carbonates and their mixtures are possibly the most studied carbonates as the second phase for composite electrolytes.

The preparation methods of the doped ceria/carbonate composite material and the sample pellet affect largely the properties of the electrolyte, e.g. the size of the particles, the homogeneity of the material and the relative density of the pellet. There are several methods to prepare the composites such as sol–gel process, co-precipitation method, hydrothermal method and glycine nitrate combustion method [6,7]. The carbonates have in practice been mixed with doped ceria either by grinding the solid powders or by suspending doped ceria in aqueous carbonate solution. There are also a few articles where a porous doped ceria structure was first fabricated and then immersed into molten carbonate [11,12]. In several XRD studies only small peaks related to the carbonate have been observed, i.e. the carbonate was mostly in amorphous form [13–15], but in some studies (XRD [16], Rietveld analysis [17]) also crystallized carbonate has been observed with some sintering methods and/or temperatures. For further details on preparing ceria-based materials and sample pellets, we refer to Refs. [4,6,7,18].

It is well-known that doped ceria is a thermally activated oxygen ion conductor where the ions hop between the vacancies, and the molten carbonate is by itself a carbonate ion conductor. In many of the articles reviewed here, a volume ratio of carbonate to doped ceria of around 1:1 has been used. This means that a continuous carbonate and/or doped ceria structure could exist throughout the composite through which the ions can move. On the other hand, it has also been argued that the carbonate forms a layer around the doped ceria particles [13,19], which may influence the overall ionic conductivity. Furthermore, it has been shown that the composite conducts protons (H^+) as well. It has been proposed that the protons move along the interface between the doped ceria and the carbonate or by hopping between the carbonate ions [4,6,15,20,21], but the hydroxyl groups are also suggested to contribute to the H^+ conductivity, especially if wet gases were used [22–24]. Additionally, under reducing conditions and at elevated temperatures (~600 °C or higher) cerium ions can be partially reduced from Ce^{4+} into Ce^{3+} [10]. This causes n-type electronic conductivity turning the doped ceria into a mixed electron/ion conductor, and the consequent lattice expansion may cause mechanical failures [10]. It should also be noted that through a simultaneous H^+ and O^{2-} conductivity, it is possible for the ions to combine in the electrolyte. This does not affect the current going through the fuel cell as electrons have already been transported through an outer circuit, but the reaction products (water and hydroxyl ions) could cause cracking or other problems inside the electrolyte.

In most of the articles reviewed here, the particle size of the doped ceria/carbonate composite is in the submicron range and often less than 100 nm. When the size of the particles is decreased to a submicrometer scale, the grain surface to volume ratio increases significantly and the surface properties become more pronounced. Possible impurities can also segregate to the boundaries adding extra contribution to the total resistance [10,25], and an increased amount of surface defects may influence both ionic and electronic conductivity [25]. Additionally, the sintering time and method (e.g. pressureless and spark plasma sintering) affect the quality and the nature of the grain boundary framework and ultimately the total conductivity [18]. A common feature of nanostructures is that the particles can agglomerate easily, which may affect the long term stability of the composite. However, short and long-term stability studies indicate that the carbonates could increase the stability of the nanocomposite [6,26–28], but care has to be taken so that the ions from the electrode do not deteriorate the electrolyte [29]. It is also possible for the (molten) carbonate phase to deteriorate during the operation but stable performance has been achieved for 200 h when CO_2 was supplied to both sides of the cell [30].

A recent development of a fuel cell with a composite electrolyte includes a so-called single layer fuel cell (SLFC; also called the electrolyte free or single component fuel cell) [31–37]. This is a new kind of fuel cell that, in contrast to standard fuel cells, does not have a well defined electrolyte layer. Instead, the SLFC has only one, more or less uniform layer composed of a mixture of electrode and electrolyte materials, but its power density is still comparable to that of three-component fuel cells [31–34]. It is possible that, even though the boundaries between the materials are more complex than in a traditional fuel cell, the electrolyte layer still exists between the anode and cathode sides. It has also been proposed that the operation of the SLFC is based on the semiconductor properties of the material [37]. In other words, the theoretical basis of SLFC is not yet fully understood and more research still needs to be done.

3. General remarks on measuring the conductivity of composite electrolytes

In order to improve the performance of the fuel cell, it is important to understand the ion transport mechanisms in the

electrolyte. Therefore ionic conductivity measurements are critical, and several methods are currently available to determine the ionic conductivity of the electrolyte such as impedance, constant current and product analysis techniques [2,38]. Unfortunately, the results from these techniques are not always consistent. For example, the quality and positioning of the electrodes affect the active area of the sample and therefore also the conductivity values. Besides, as the properties of the cell are affected by the gas atmosphere, the conductivity measurements are often done both in cathode (e.g. air) and anode (e.g. hydrogen) atmospheres.

In conductivity measurements both voltage and current over the sample are measured. The electrochemical reactions can be controlled with current and the reaction sites are called electrodes. Thus the current wires are always attached on the electrodes. Depending on the position of the voltage probes, the measurement system is either called a 2, 3 or 4-point system. In the 2-point system both voltage probes are attached on the electrodes, while in 3 and 4-point systems one and two voltage probes, respectively, are directly attached on the electrolyte. Only a minuscule current should pass through the voltage probes i.e. contributions of one and two electrodes can be neglected in 3 and 4-point systems, respectively. However, in 2 and 3-point system measurements the current and potential probe(s) can use the same wire(s), in which case the effect of the wire(s) has to be taken into account. Additionally, the physical position of the probes is important as it affects the voltage distribution and will be discussed later in connection with the constant current measurements. To our knowledge, mainly 2-point system has been used for measuring the conductivity of the LT-SOFC composite electrolytes, but also 4-point system has been employed in some of the constant current measurements.

Another way to measure the conductivity of the electrolyte would be to use samples with different electrolyte thicknesses while keeping the rest of the system unchanged. The difference in the losses in the electrolyte should then be directly proportional to the differences in the electrolyte thicknesses i.e.

$$R_{\mathrm{Total}} = R_{\mathrm{Electrolyte}} + R_{\mathrm{Other}} = \frac{1}{\sigma A}\cdot L + R_{\mathrm{Other}} \quad (1)$$

where R_{Total}, $R_{\mathrm{Electrolyte}}$ and R_{Other} are the total resistance of the measurement system, the resistance of the electrolyte and the resistance of the other parts, respectively, and σ, A and L are the conductivity, area and length of the electrolyte, respectively. Unfortunately, this method is quite time-consuming as it needs several measurements with the same electrolyte, and has thus seldom been used for LT-SOFC electrolytes.

The following form of the Arrhenius equation [1] is often used to represent the dependence of the temperature on the ionic conductivity of the doped ceria/carbonate composite

$$\sigma T = A \exp\left(\frac{-E_a}{k_B T}\right) \quad (2)$$

where σ is the conductivity of the electrolyte, T is the temperature, A is a scaling factor (usually a constant but can, for example, be a function of temperature), E_a is the activation energy and k_B is the Boltzmann constant. If the scaling factor and the energy related to the conduction mechanisms remain constant, then $\ln(\sigma T)$ vs. $1/T$ is a linear function, which we use to denote as the linearity of the conductivity. The activation energy may change around the melting point of the carbonate mixture but the conductivity is generally linear before and after the change, as will be shown later.

This article focuses on doped ceria and carbonate composites (Li_2CO_3, Na_2CO_3 and K_2CO_3) with several different mixing ratios. Later we will show that the conductivity increases often rapidly around the melting point of the carbonate mixture. Thus, the melting points of Li_2CO_3, Na_2CO_3 and K_2CO_3 mixtures are relevant to LT-SOFCs and the melting points of pure carbonates and their eutectic compositions are shown in Table 1. The ratio between the doped ceria and the carbonate is also one of the significant parameters that affect the properties of the composite. As different mixing methods have been adopted, different ratios (weight, volume and molar) are used when reporting the results. To make a straightforward comparison easier, we show the conversion of these ratios for one eutectic sample in Table 2.

The specific features of the conductivity measurement techniques (impedance, constant current and product analysis) used with composite electrolytes will be discussed in Sections 4–6. It should also be noted, that most of the conductivity values for LT-SOFC composite electrolytes shown in this paper are taken directly from the graphs as numerical values are missing, which may cause some extra uncertainty. Additionally, in a few articles we found that the total ionic conductivity has been derived directly from the I–V curves, often without adequate consideration of different loss mechanisms. This raises a large uncertainty as only a part of the ohmic resistance and other contributions can be attributed to the electrolyte resistance. Thus only approximate values for the ionic conductivity can be attained when they are determined from the I–V curves. Moreover, there have been a few EMF (electromotive force) measurements conducted on the doped ceria and the doped ceria/carbonate electrolytes [39–41]. In these measurements different gas conditions are applied on the electrodes. The ions will then diffuse to the other side until the electric field due to the accumulation of the ions will stop the (macroscopic) diffusion. It is possible to measure the transport number of the specific ions and electrons (but not the actual conductivities) if the reactions and losses due to the reactions are known. As only a few EMF measurements have been performed recently, they are not further discussed in this article. More information about the EMF measurements can be found in Refs. [42,43].

4. Impedance measurements on doped ceria based composite materials

4.1. Theoretical fundamentals

Electrochemical impedance spectroscopy (EIS), or simply impedance measurement, is based on applying an external stimulus to the cell and then measuring its response, e.g. a sinusoidal AC voltage over a range of frequencies [44,45]. In theory, the response should be a sinusoidal current whose amplitude and phase shift compared to the voltage depends on the sample properties, e.g. charge transfer and conductivity. In impedance measurements, the I–V curve is linearized around a specific voltage/current point and unless the curve is linear around the specific point, the amplitude of the stimulus should be as small as possible to ensure accurate results [44,45]. Fortunately, at increased temperatures the activation

Table 1
Melting points of lithium, sodium and potassium carbonates and some of their eutectic mixtures.

M_2CO_3 (mol%)			Melting	Ref.
Li	Na	K	Point (°C)	
100			723	[65]
	100		851	[65]
		100	891	[65]
52	48		501	[83]
62		38	488	[83]
43.5	31.5	25	397	[83]

Table 2
An example of doped ceria/carbonate ratios. The weight to volume ratio is from Ref. [21] and the weight to molar ratio was calculated using the molar masses.

SDC = $Ce_{0.8}Sm_{0.2}O_{1.9}$		
LNK = $(Li_{0.435}Na_{0.315}K_{0.25})_2CO_3$		
Weight	Volume	Molar
SDC:LNK	SDC:LNK	SDC:LNK
90:10	74.5:25.5	83.9:16.1
70:30	43.1:56.9	57.5:42.5
50:50	24.5:75.5	36.7:63.3

losses decrease due to faster reaction kinetics [2] and the *I–V* curve is mostly linear at high temperature i.e. the electrolyte resistance is practically linear. The EIS data is mostly shown as a Nyquist plot and the ionic conductivity and/or the electrode contributions can be determined from the semicircles in the plot. In practice, equivalent circuits are used to estimate the contribution of different parts of the sample but care has to be taken in choosing a correct circuit and a fitting algorithm to minimize the analysis errors. For example, if conduction mechanisms of a sample cell change around some specific temperature, different equivalent circuits may represent the cell below and over that temperature point. More detailed description of the EIS analysis can be found in Refs. [44,45].

The size of the electrolyte particles affects the conductivity of the ceramic electrolyte. For example, EIS data of YSZ particles with different sizes were compared in Ref. [25] and typical EIS Nyquist plots for a single and multiple YSZ crystal samples are given in Fig. 1. A single crystal sample shows only a bulk and an electrode semicircle. However, with multiple crystal samples, usually three semicircles are seen, where the high frequency semicircle is attributed to bulk conductivity, the medium frequency to grain boundary conductivity and the low frequency to electrode contributions. As the particle size decreases, the timescales of the different ion conductions start to overlap and cannot be distinguished from each other. With particle sizes larger than 1 μm, the grain boundary and electrode semicircles seemed to combine as the particle size was decreased. However, in the thin film electrolyte (particle size 10 nm) the bulk and grain boundary semicircles were assumed to combine together. The grain and grain boundary semicircles are quite commonly assumed to combine with each other also with other nanoparticle SOFC electrolyte materials, but whether this is actually true has not been studied completely. Nevertheless, as the doped ceria particles (e.g. SDC and GDC) have a similar crystal structure to YSZ [1], the same kind of EIS characteristics related to the particle size can be assumed to apply both to YSZ and doped ceria. Additionally, in a typical composite material that is used as the LT-SOFC electrolyte, there exists several different ion conducting mechanisms (e.g. H^+, O^{2-}, CO_3^{2-}). When the number of conduction mechanisms increases and more semicircles overlap each other, the determination of the specific ion conductivities becomes even harder.

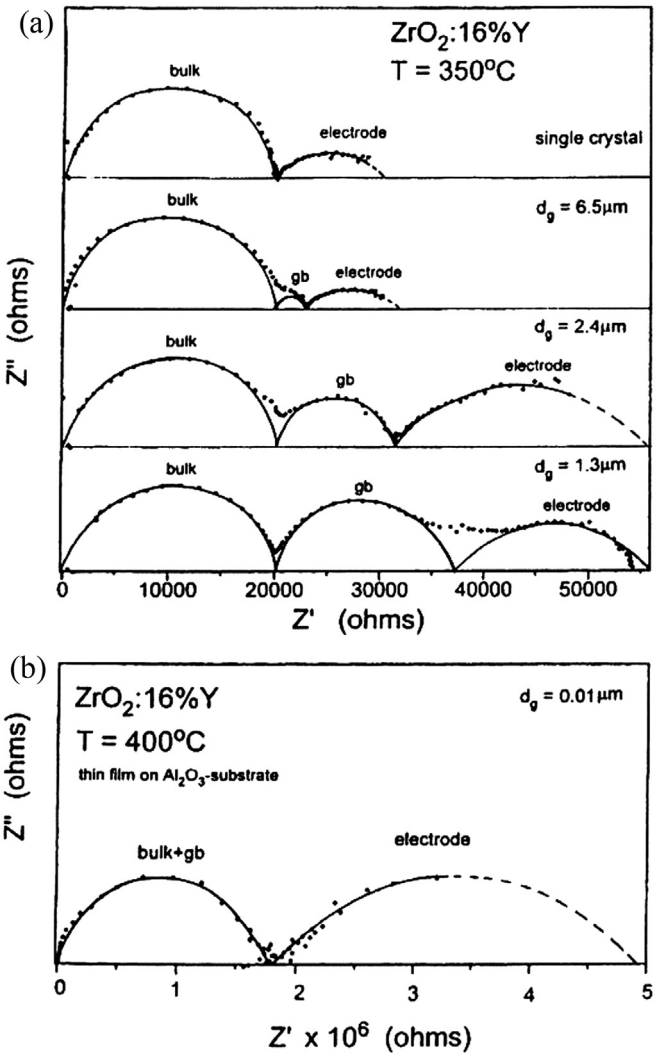

Fig. 1. Complex impedance spectra obtained for (a) single crystal and microcrystalline YSZ bulk specimens and (b) for nanocrystalline YSZ films. Reproduced from Ref. [46] by permission of ECS, The Electrochemical Society, Copyright 1998.

4.2. Results

The conductivity of the doped ceria/carbonate composite electrolytes has mostly been measured with EIS. General parameters that have been used with the measurements (amplitude, frequency range and electrode type) are shown in Table 3 while the data from recent results is summarized in Table 4. This section is divided into two subsections: the measurement parameters and the effect of the carbonates. It can be pointed out that the highest conductivity at 650 °C, 1.1 S cm^{-1} (the only one of the LT-SOFC electrolytes to be over 1 S cm^{-1} at that temperature), has been measured for a sample, in which $Ce_{0.8}Sm_{0.2}O_{1.9}$ was mixed with $(Li_{0.52}Na_{0.48})_2CO_3$ with a weight ratio of 50:50 [47]. Unfortunately, no fuel cell measurements were conducted for the electrolyte so the real performance in an operating fuel cell is unknown. Additionally, in some of the articles the power density of a complete cell was measured as well in addition to the conductivity of the electrolyte. In several of them, power densities of 1 W cm^{-2} or higher were also recorded at temperatures around 600 °C [3,48–50]. Unfortunately, the thickness of the electrolyte is not always mentioned and the effect of different gas atmospheres, electrodes and cell preparation methods make the comparison of the composite electrolytes problematic for real fuel cell conditions.

4.2.1. The measurement parameters

The transport processes can in theory be attributed to the semicircles but in practice the determination of the conductivities is not always simple, especially with nanocomposites. In the reviewed articles, one or two semicircles are attributed to ionic conductivities at low temperatures (300 °C–400 °C). If the frequency range is wide enough, the electrode contribution can sometimes also be observed. It should also be noted that as the temperature is increased, the timescales of the semicircles

Table 3
Measurement parameters.

Method			Ref.
Ampl. mV	Freq. range	Electrode	
n/a	n/a	Ag	[84]
5	1 Hz–100 kHz	Ag	[21]
n/a	n/a	Ag	[14]
20	0.5 Hz–50 kHz	n/a	[16]
n/a	n/a	Ag	[48]
n/a	n/a–1 MHz	Au	[22]
10	0.1 Hz–100 kHz	Ag	[15]
	IV	Elec. + Ag	[15]
10	0.1 Hz–1 MHz	Ag	[67]
n/a	n/a	Au	[54]
1000	20 Hz–1 MHz	Au	[56]
10	0.1 Hz–1 MHz	Ag	[63]
n/a	100 Hz–13 MHz	n/a	[17]
10	0.1 Hz–100 kHz	Ag	[62]
10	0.01/10 Hz–8 MHz	Ag	[51]
100	0.01 Hz–1 MHz	Ag	[29]
20	5 Hz–13 MHz	Ag	[13]
n/a	0.1 Hz–1 MHz	n/a	[49]
n/a	n/a	Ag	[11]
10	0.1 Hz–1 MHz	Ag	[12]
5	1 Hz–100 kHz	Ag	[3]
	IV	Elec. + Ag	[3]
5	5 Hz–13 MHz	Ag	[55]
10	0.1 Hz–100 kHz	n/a	[64]
	IV	Elec. + Ag	[64]
10	0.1 Hz–100 kHz	Ag	[53]
10	0.05 Hz–100 kHz	Au/Ni	[52]
10	0.1 Hz–100 kHz	Ag	[39]
n/a	n/a	n/a	[50]
	IV	Elec.	[50]
10	0.1 Hz–100 kHz	Elec. + Ag	[85]
n/a	0.1 Hz–1 MHz	Ag	[60]
10	0.01 Hz–1 MHz	Ag	[61]
10	0.01 Hz–100 kHz	Ag	[86]
	IV	Elec.	[86]
10	0.03 Hz–50 kHz	Au	[47]

decrease, i.e. the high frequency semicircles start disappearing and the low frequency semicircles start appearing at increased temperatures. When going beyond the melting point of the composite, the remaining semicircles and/or the emerging tail are mostly attributed to the electrode or mass transfer mechanisms and the ionic conductivity at high temperatures is measured from the high frequency interception with the *x*-axis (real part of the resistance) [12,29,39,47,51–54]. However, different preparation methods [53,55] and low amounts of carbonates [14] can lead to a situation where the grain boundary semicircle is visible even at high temperatures. Unfortunately, the other reviewed articles exclude the information at which point the electrolyte conductivity is defined.

The strength of the stimulus (applied AC voltage) affects the nonlinear part of the sample resistance. Generally the used stimulus ranged from 5 mV to 20 mV but also 100 mV [29] and 1 V amplitudes [56] have been used. The effect of the amplitude on the Nyquist plot has been examined at temperatures below (Fig. 2) [16] and over the melting point of the carbonates [22]. It was observed that the high frequency arc (seen only as the ohmic part in Ref. [22]) was insensitive to the changes in the magnitude while the low frequency arc changed as the amplitude was increased. As the electrolyte resistance is almost linear at operating temperatures, small and large stimuli should give the same kind of response for the electrolyte [2]. Thus the unchanging high frequency contribution can be attributed to the ionic conductivity. On the other hand, electrochemical reactions are nonlinear and the changing low frequency arc can thus be attributed to the electrodes. Therefore it should be possible to determine the electrode contributions from the electrolyte contributions using different amplitudes even though the electrode contribution would overlap with the electrolyte conductivity.

In addition to the stimulus (and the gas atmosphere), the electrode reactions are naturally dependent on the catalyst material. The most common electrode has been silver paint, but also gold [47,51,52,56,57], nickel [51,52], and platinum [58] based electrodes have been reported. In Ref. [51] Ag, Au, $LiNiO_x$ composite and Ni composite electrodes in different atmospheres were compared (Fig. 3). At 600 °C the high frequency 8 MHz intercept with the real axis remained practically constant with the different electrodes while only the size of the semicircles changed. This may imply that at higher temperatures (over the melting point) the total conductivity could be measured using the high frequency intercept. Additionally, the $LiNiO_x$ composite showed the lowest electrode resistance among the measured electrodes in air and CO_2–O_2 atmospheres while Ni composite electrodes showed the lowest resistance in wet H_2 atmosphere. Au had the highest resistance of the electrodes while the resistance from Ag was in between of these values. The EIS semicircles due to the electrode reactions could in principle be neglected in the 4-point method assuming that the artifacts due to the connections have been taken into account [59]. To our knowledge, a four-probe configuration was mentioned only in Ref. [47], while in the other articles the 2-point EIS method was used to measure the conductivity of the composite electrolyte. However, it was not clear how the voltage probes were actually attached to the sample i.e. in fact a 2-point method may have been used in Ref. [47].

In every article where EIS was used, the samples were measured at least either in air or in other oxygen rich atmospheres, but the effect of the gas atmospheres has also been studied in several articles. For example, the effect of carbon dioxide on the conductivity of the composite electrolyte has been measured using different partial pressures of CO_2 (along with other gases), and it was observed that the difference in the conductivity values was minimal or even negligible [3,11,47,51,52]. The conductivity has also been measured with nonreactive gases such as argon [39] and nitrogen [50], and the difference compared to air was noted to be nonexistent. These results may imply that the conductivity of "internal species" (practically oxygen and carbonate ions) is not largely affected by the atmosphere, at least if no reducing atmosphere (e.g. hydrogen) is used.

On the other hand, the effect of the hydrogen atmosphere on the conductivity of the gadolinium and samarium doped ceria/carbonate composites, is harder to analyze as the measurements range significantly from each other: At high temperatures, the conductivity in hydrogen rich atmosphere was noted to be 10% to 40% higher than in oxygen rich atmosphere [11,39], the conductivity in pure hydrogen was 30% higher than in other atmospheres, including wet hydrogen [50], the conductivity in H_2/CO_2 atmosphere was several times higher than in dry and wet air, but similar to the values in pure O_2 and $O_2/CO_2/N_2$ atmospheres [52] and the conductivity was noted to be several times higher in hydrogen rich atmospheres compared to oxygen rich atmospheres [47]. Additionally, in Ref. [51] the conductivity of a composite sample was measured in air, CO_2/O_2 and in wet H_2. Even though the semicircles were not similar in the different atmospheres, the high frequency interception in the Nyquist curves was reported to be practically the same, i.e. the conductivity differences were reported to be negligible. Only at 650 °C the conductivity in reducing atmospheres was reported to be higher, which was assumed to be due to increased electronic conductivity. In similar ways the temperature at which point the rapid increase in the conductivity appears, ranges from each other: In Refs. [39,50,52] the increase in hydrogen rich atmosphere appears at temperatures lower than in other

Table 4
Summary of the EIS measurements.

Materials						Conductivity							Power density		Ref.
Oxide		Spec.	M_2CO_3 (mol%)			Gases	Max S cm^{-1}	T °C	σ S cm^{-2}	T °C	Slope change	Temp. range	Max mW cm^{-2}	T °C	
Formula	Amount		Li	Na	K										
$Ce_{0.8}Gd_{0.2}O_{1.9}$	90 wt	600 °C[a]	53	47		n/a	6.8e-2	650	4.4e-2	550	550	400–700			[84]
	85 wt	600 °C[a]	53	47		n/a	8.3e-2	650	7.9e-2	550	500	350–650			
	80 wt	600 °C[a]	53	47		n/a	1.3e-1	700	1.1e-1	550	525	350–700			
	75 wt	600 °C[a]	53	47		n/a	1.6e-1	700	1.6e-1	550	475	375–700			
	70 wt	600 °C[a]	53	47		n/a	7.8e-2	600	5.9e-2	550	550	400–600			
	65 wt	600 °C[a]	53	47		n/a	1.0e-1	650	9.9e-2	550	550	400–650			
	90 wt	650 °C[a]	100			n/a	1.6e-1	700	4.1e-2	550	550	400–700			
	80 wt	650 °C[a]	100			n/a	1.3e-2	700	2.0e-3	550	500	400–700			
	75 wt	650 °C[a]	100			n/a	3.7e-2	700	5.4e-3	550	No	400–700			
	70 wt	650 °C[a]	100			n/a	3.1e-2	700	4.6e-3	550	No	400–700			
	65 wt	650 °C[a]	100			n/a	1.2e-1	600	9.8e-2	550	550	400–650			
	90 wt	650 °C[a]		100		n/a	3.1e-3	700	5.1e-4	550	No	400–700			
	85 wt	650 °C[a]		100		n/a	3.8e-2	700	1.1e-3	550	No	400–700			
	80 wt	650 °C[a]		100		n/a	4.6e-4	650	1.0e-4	550	No	400–650			
	70 wt	650 °C[a]		100		n/a	9.3e-4	700	1.5e-4	550	No	400–700			
$Ce_{0.8}Sm_{0.2}O_{1.9}$	100 wt					Air	8.0e-3	650	1.6e-3	550	No	300–650			[21]
	90 wt		43.5	31.5	25	Air	1.8e-2	650	1.2e-2	550	350	300–650	550[b]	650	
	70 wt		43.5	31.5	25	Air	6.4e-2	650	5.4e-2	550	375	300–650	720[b]	650	
	50 wt		43.5	31.5	25	Air	1.5e-1	650	1.4e-1	550	400	300–650	573[b]	650	
$Ce_{0.8}Gd_{0.2}O_{1.9}$	90 wt		53	47		Air	1.3e-1	800	7.0e-2	550	550	400–800			[14]
	80 wt		53	47		Air	2.1e-1	800	1.1e-1	550	550	400–800			
	75 wt		53	47		Air	2.1e-1	800	1.7e-1	550	550	400–800	92[c]	550	
	70 wt		53	47		Air	2.3e-1	800	1.7e-1	550	525	400–800			
	65 wt		53	47		Air	1.0e-1	800	3.1e-2	550	550	400–800			
$Ce_{0.9}G_{0.1}O_{1.95}$	80 wt		72.7		27.3	Air	1.4e-1	690	7.9e-2	550	570	300–700			[16]
	70 wt		72.7		27.3	Air	1.8e-1	660	1.1e-1	550	570	300–700			
	60 wt		72.7		27.3	Air	6.6e-1	690	2.2e-1	550	570	300–700			
$Ce_{0.8}Sm_{0.2}O_{1.9}$	100 wt		53	47		Air	2.0e-2	625	9.4e-3	550	No	400–625			[48]
	90 wt		53	47		Air	2.7e-2	625	1.6e-2	550	475	400–625	435[c]	600	
	85 wt		53	47		Air	5.0e-2	625	4.2e-2	550	475	400–625	679[c]	600	
	80 wt		53	47		Air	7.8e-2	625	7.5e-2	550	450	400–625	949[c]	600	
	75 wt		53	47		Air	1.0e-1	625	8.7e-2	550	475	400–625	1085[c]	600	
	70 wt		53	47		Air	9.8e-2	625	8.7e-2	550	475	400–625	890[c]	600	
	65 wt		53	47		Air	1.3e-1	625	1.2e-1	550	475	400–625	885[c]	600	
$Ce_{0.8}Gd_{0.2}O_{1.9}$	50 vol		67	33		Air	1.9e-1	625	8.2e-2	550	480	425–625			[22]
	50 vol		52	48		Air	1.3e-1	625	7.1e-2	550	480	425–625			
	50 vol		33	67		Air	1.2e-1	625	6.0e-2	550	480	425–625			
$Ce_{0.8}Sm_{0.2}O_{1.9}$	100 wt					Air	1.6e-2	600	9.4e-3	550	No	400–600			[15]
	80 wt		50	50		Air	4.7e-2	600	4.1e-2	550	475	400–600			
	80 wt		50		50	Air	5.0e-2	600	4.1e-2	550	450	400–600			
	80 wt			50	50	Air	6.7e-3	600	2.9e-3	550	No	400–600			
	80 wt	*I–V*	50	50		H_2/air	9.3e-2	600	7.1e-2	500	n/a	500 & 600	600[e]	600	
	80 wt	*I–V*	50		50	H_2/air	9.2e-2	600	6.7e-2	500	n/a	500 & 600	550[e]	600	
	80 wt	*I–V*		50	50	H_2/air	8.3e-2	600	4.4e-2	500	n/a	500 & 600	550[e]	600	
$Ce_{0.8}Sm_{0.2}O_{1.9}$	100 wt					Air	3.6e-3	600	1.8e-3	550	No	450–600	147[e]	600	[67]
	80 wt		52	48		Air	3.9e-1	600	4.1e-1	550	500	450–600	532[e]	600	
	80 wt		52		48	Air	1.7e-1	600	1.6e-1	550	475	450–600	410[e]	600	
	80 wt			48	52	Air	1.2e-2	600	2.5e-3	550	No	450–600	373[e]	600	
$Ce_{0.8}Sm_{0.2}O_{1.9}$	70 wt			100		Air			1.6e-3	550	No	200–550			[54]
	70 wt		67	33		Air			3.5e-1	550	500	200–550			
CeO_2	100 vol					Air	1.2e-4	625	4.0e-5	566	No	225–625			[56]
Al_2O_3	100 vol					Air	4.3e-8	625	2.4e-8	566	No	425–625			
TZP	100 vol					Air	3.2e-3	625	1.4e-3	566	No	275–625			
$Ce_{0.8}Gd_{0.2}O_{1.9}$	100 vol					Air			1.0e-2	566	No	225–n/a			
Carbonate	100 vol		33	67		Air			2.5e-1	490	No	n/a–490			
CeO_2	50 vol		33	67		Air	2.3e-1	625	1.3e-1	566	475	225–625			
Al_2O_3	50 vol		33	67		Air	5.5e-4	625	2.8e-4	566	No	225–625			
TZP	50 vol		33	67		Air	2.0e-2	625	1.9e-2	566	525	225–625			
$Ce_{0.8}Gd_{0.2}O_{1.9}$	50 vol		33	67		Air			5.6e-2	566	500	225–600			
$Ce_{0.8}Sm_{0.2}O_{2-\delta}$	80 wt	675 °C[d]	53	47		Air	9.1e-2	600	5.3e-2	550	No	300–600			[63]
$Ce_{0.8}Gd_{0.2}O_{2-\delta}$	80 wt	675 °C[d]	53	47		Air	5.8e-2	600	3.1e-2	550	No	300–600			
$Ce_{0.8}Y_{0.2}O_{2-\delta}$	80 wt	675 °C[d]	53	47		Air	3.1e-2	600	1.7e-2	550	No	300–600			
$Ce_{0.8}Gd_{0.2}O_{1.9}$	100 wt					Air	3.9e-3	575	2.4e-3	550	No	300–575			[17]
	95 wt		67	33		Air	9.2e-3	575	7.4e-3	550	500	300–575			
	80 wt		67	33		Air	7.1e-2	575	4.7e-2	550	475	300–575			
	60 wt		67	33		Air	1.1e-1	575	6.8e-2	550	500	300–575			
Alumina	95 wt		67	33		Air	3.4e-4	600	1.2e-4	550	No	350–600			
	80 wt		67	33		Air	2.1e-2	600	1.2e-3	550	No	350–600			
	60 wt		67	33		Air	1.2e-1	600	6.8e-2	550	500	350–600			
$Ce_{0.9}Gd_{0.1}O_{2-\delta}$	45 vol		62		38	Air	3.2e-1	650	1.9e-1	550	490	400–650			[51]
Carbonate	100 vol		62		38	Air			6.0e-1	490	No	390–490			

Materials							Conductivity							Power density		Ref.
Oxide		Prep. method	Spec.	M_2CO_3 (mol%)			Gases	Max S cm^{-1}	T °C	σ S cm^{-1}	T °C	Slope change	Temp. range	Max mW cm^{-2}	T °C	
Formula	Amount			Li	Na	K										
$Ce_{0.8}Sm_{0.2}O_{1.9}$	75 wt					100	Air	1.8e-1	700	1.9e-2	550	650	400–700	602[m]	700	[62]
$Ce_{0.8}Gd_{0.05}Y_{0.15}O_{1.9}$	60 wt			52	48		Air			2.6e-1	550	n/a	550			[29]
$Ce_{0.8}Sm_{0.2}O_{1.9}$	80 wt				100		Air	3.5e-1	575	3.5e-1	550	325	125–575	800[m]	550	[13]
$Ce_{0.8}Sm_{0.1}Ca_{0.1}O_{2-\delta}$	n/a				100		Air	4.5e-1	600	4.0e-1	550	400	300–600	980[m]	560	[49]
$Ce_{0.8}Sm_{0.2}O_{1.9}$	70 vol	ST[f]		52	48		Air	3.5e-1	650	2.5e-1	550	490	400–650			[11]
	65 vol	ST[f]		52	48		Air	4.3e-1[l]	650	2.9e-1[l]	550	500[l]	400–650			
	60 vol	ST[f]		52	48		Air	5.3e-1	650	3.8e-1	550	500	400–650			
	65 vol	ST[f]		52	48		$CO_2 + O_2$	3.4e-1	650	2.4e-1	550	500	400–650			
	65 vol	ST[f]		52	48		Air	3.5e-1[l]	650	2.4e-1[l]	550	490[l]	400–650			
	65 vol	ST[f]		52	48		Wet H_2	3.8e-1	650	3.0e-1	560	500	400–650			
$Ce_{0.8}Sm_{0.2}O_{1.9}$	n/a	MSI[g]		52	48		Air	1.1e-1	625	8.7e-2	550	500	350–625			[12]
	n/a	MP[g]		52	48		Air	5.5e-2	625	2.4e-2	550	500	350–625			
$Ce_{0.8}Sm_{0.2}O_{1.9}$	100 wt	n/a					Air	1.6e-2	650	5.2e-3	550	No	300–650			[3]
	70 wt	GN[h]		50	50		Air	1.0e-1	650	7.9e-2	550	500	300–650	607[n]	650	
	70 wt	OC[h]		50	50		Air	1.5e-1	650	1.1e-1	550	500	300–650	1266/1704[o]	650	
	70 wt	SG[h]		50	50		Air	1.6e-1	650	1.2e-1	550	500	300–650	1121[n]	650	
	70 wt	OC[h]		50	50		$CO_2 + O_2$	1.6e-1	650	1.3e-1	550	500	300–650			
	70 wt	OC[h]	*I–V*	50	50		H_2/air	9.7e-2	650	4.5e-2	550	500	300–650			
	70 wt	OC[h]	*I–V*	50	50		$H_2/CO_2 + O_2$	1.4e-1	650	6.1e-2	550	500	300–650			
$Ce_{0.8}Sm_{0.2}O_{1.9}$	80 wt	μm[i]		n/a	n/a		n/a			1.1e-2	525	500	250–550			[55]
	80 wt	Semi μm[i]		n/a	n/a		n/a			1.6e-2	550	500	250–550			
	30 mol	nm[i]		n/a	n/a		n/a			1.9e-2	525	500	250–550			
$Ce_{0.8}Sm_{0.2}O_{1.9}$	80 wt	pH4[j]		53	47		n/a	4.6e-2	750	8.0e-3	550	No	400–750			[64]
	80 wt	pH6[j]		53	47		n/a	5.0e-2	750	1.1e-2	550	No	400–750			
	80 wt	pH8[j]		53	47		n/a	2.4e-2	750	3.4e-3	550	No	400–750			
	80 wt	pH4[j]	*I–V*	53	47		H_2/air	6.1e-1	600	4.9e-1	550	No	450–600			
	80 wt	pH6[j]	*I–V*	53	47		H_2/air	6.4e-1	600	5.0e-1	550	No	450–600	817[m]	600	
	80 wt	pH8[j]	*I–V*	53	47		H_2/air	5.6e-1	600	4.2e-1	550	No	450–600			
$Ce_{0.8}Sm_{0.2}O_{1.9}$	80 wt	SR[k]		52	48		Air	1.5e-1	600	1.1e-1	550	525	300–600	696[p]	600	[53]
	80 wt	CN[k]		52	48		Air	2.0e-1	600	1.5e-1	550	500	300–600	825[p]	600	
	33 mol	NANO		52	48		Air	1.8e-1	600	1.4e-1	550	500	300–600	839[p]	600	

Materials						Conductivity							Power density		Ref.
Oxide		Spec.	M_2CO_3 (mol%)			Gases	Max S cm^{-1}	T °C	σ S cm^{-1}	T °C	Slope change	Temp. range	Max mW cm^{-2}	T °C	
Formula	Amount		Li	Na	K										
$Ce_{0.9}Gd_{0.1}O_{1.95}$	80 wt		72.7		27.3	Dry air	3.4e-1	660	1.3e-1	550	500	395–660			[52]
	80 wt		72.7		27.3	A[r]	4.0e-1	670	1.5e-1	540	485	395–670			
	80 wt		72.7		27.3	C[r]	3.8e-1	660	1.6e-1	550	500	395–660			
	70 wt		72.7		27.3	Dry air	2.4e-1	610	1.8e-1	550	500	300–610	58.8[u]	550	
	70 wt		72.7		27.3	O_2	6.5e-1	610	4.3e-1	550	500	335–610			
	70 wt		72.7		27.3	Wet air	2.3e-1	610	1.6e-1	550	500	335–610			
	70 wt		72.7		27.3	C[r]	6.3e-1	610	3.5e-1	550	500	300–610			
	70 wt		72.7		27.3	A[r]	6.3e-1	610	5.2e-1	550	415	300–610			
	70 wt		72.7		27.3	C + A[r]	9.8e-1	650	6.3e-1	550	500	300–650			
$Ce_{0.8}Sm_{0.2}O_{1.9}$	80 wt		52	48		Air	5.6e-1	600	4.4e-1	550	490	450–600	590[v]	600	[39]
	80 wt		52	48		Argon	5.6e-1	600	4.5e-1	550	490	450–600			
	80 wt		52	48		H_2	7.7e-1	600	5.7e-1	550	470	450–600			
$Ce_{0.8}Sm_{0.2}O_{1.9}$	100 wt					Air	1.6e-2	600	9.4e-3	550	No	400–600			[50]
	80 wt		53	47		N_2	8.4e-2	600	8.3e-2	550	440	400–600			
	80 wt		53	47		$N_2 + H_2O$	8.4e-2	600	8.3e-2	550	420	400–600			
	80 wt		53	47		Air	8.4e-2	600	8.3e-2	550	450	400–600			
	80 wt		53	47		Air + H_2O	8.4e-2	600	8.3e-2	550	450	400–600			
	80 wt		53	47		H_2	1.1e-1	600	1.1e-1	550	400[t]	400–600			
	80 wt		53	47		$H_2 + H_2O$	8.4e-2	600	8.3e-2	550	400[t]	400–600			
	70 wt		67	33		$H_2 + H_2O$	1.1e-1	600	1.1e-1	550	475	400–600			
	70 wt	*I–V*	67	33		H_2/air	1.9e-1	600	1.5e-1	550	No	400–600	1100[v]	600	
$Ce_{0.8}Sm_{0.2}O_{1.9}$	33 mol	700 °C[q]		100		Air/air			2.7e-2	550	No	350–550			[85]
	33 mol	700 °C[q]		100		H_2/air			3.0e-2	550	No	350–550	375[v]	550	
$Ce_{0.8}Ca_{0.2}O_{1.9}$	30 mol			50	50	Air	9.0e-2	600	6.2e-2	550	No	400–600	567[u]	550	[60]
	30 mol			50	50	H_2	1.8e-2	600	1.2e-2	550	No	400–600			
$Ce_{0.8}Sm_{0.1}Ca_{0.1}O_{2-\delta}$	n/a			100		Air	5.7e-1	650	4.5e-1	560	No	280–650	900[v]	550	[61]
	n/a			100		H_2	1.9e-1	640	1.5e-1	550	No	330–640			
$Ce_{0.8}Sm_{0.2}O_{1.9}$	80 wt		52	48		Air	2.4e-1	650	1.5e-1	550	500	300–650			[86]
	80 wt	*I–V*	52	48		Wet H_2/air	8.8e-2	600	8.2e-2	550	No	450–600	916[w]	550	
$Ce_{0.8}Sm_{0.2}O_{1.9}$	90 wt		52	48		A1[s]	1.4e-2	700	5.1e-3	525	500	400–700			[47]
	80 wt		52	48		A1[s]	3.6e-2	700	2.1e-2	550	500	400–700			
	50 wt		52	48		A1[s]	1.1e0	700	6.8e-1	550	475	400–700			
	90 wt		52	48		C3[s]	3.6e-3	700	9.3e-4	550	525	400–700			
	80 wt		52	48		C3[s]	7.3e-3	700	2.7e-3	550	525	400–700			
	50 wt		52	48		C3[s]	9.8e-1	700	7.6e-1	550	475	400–700			
	90 wt		52	48		A2[s]	8.0e-3	670	3.7e-3	550	500	400–670			

(*continued on next page*)

Table 4 (*continued*)

Materials						Conductivity							Power density		Ref.
Oxide		Spec.	M_2CO_3 (mol%)			Gases	Max S cm^{-1}	T °C	σ S cm^{-1}	T °C	Slope change	Temp. range	Max mW cm^{-2}	T °C	
Formula	Amount		Li	Na	K										
	90 wt		52	48		C1[s]	3.0e-3	670	1.3e-3	550	475	400–670			
	90 wt		52	48		C2[s]	3.0e-3	670	1.4e-3	550	475	400–670			

[a] Sintering temperature.
[b] $H_2/CO_2 + O_2$.
[c] H_2/air.
[d] Sintering temperature.
[e] H_2/Air.
[f] ST = Sacrificial template.
[g] MSI = molten salt infiltration MP = mixing-pressing.
[h] GN = glycine-nitrate combustion, OC = oxalate co-precipitation, SG = sol–gel process.
[i] Particle size.
[j] pH during the preparation of SDC.
[k] SR = solid state reaction, CN = citric acid–nitrate combustion.
[l] The conductivities in air were obtained from two different graphs.
[m] H_2/air.
[n] $H_2/CO_2 + O_2$ & thickness of the electrolyte: 0.5 mm.
[o] $H_2/CO_2 + O_2$ & thickness of the electrolyte: 0.5 mm/0.25 mm.
[p] Wet H_2/air.
[q] Sintering temperature.
[r] A = $H_2 + CO_2$ (80/20), C=$O_2 + CO_2 + N_2$ (15/10/75).
[s] A1 = $H_2 + CO_2$ (80/20), A2 = $H_2 + CO_2 + N_2$+CO (15/50/5/30), C1 = $O_2 + CO_2 + N_2$ (15/30/55), C2 = $O_2 + CO_2 + N2$ (15/70/15), C3 = $O_2 + CO_2 + N_2$ (19/10/71).
[t] The rapid increase in the conductivity occurred most likely below 400 °C.
[u] H_2/O_2.
[v] H_2/air.
[w] Wet H_2/air.

atmospheres, while in Refs. [11,47] the relative position of the increase depends on the partial pressures of H_2, O_2, N_2, CO_2 and CO in a more arbitrary way. In summary, the hydrogen rich atmosphere may increase the conductivity in the aforementioned gadolinium or samarium doped ceria/carbonate composites but no other generalization can be easily done.

In addition to the gadolinium and samarium doped ceria/carbonate composites, also $Ce_{0.8}Ca_{0.2}O_{1.9}/NaKCO_3$ composites [60] and $Ce_{0.8}Sm_{0.1}Ca_{0.1}O_{2-\delta}/Na_2CO_2$ composites [61] were measured in air and hydrogen atmospheres. Opposite to the SDC and GDC carbonate composites, the conductivity in air was several times larger than in hydrogen, and the conductivity slope both in air and H_2 showed no change in the measurement range. The reason for the higher conductivity in air compared to hydrogen was not explained. Additionally, the activation energy of the composite was very low (0.283 eV in air) in Ref. [61] producing high conductivities in air and hydrogen even at low temperatures (0.1 S cm^{-1} and 0.08 S cm^{-1} at 280 °C, respectively). $Ce_{0.8}Sm_{0.1}Ca_{0.1}O_{2-\delta}/Na_2CO_3$ composite samples were also prepared in Ref. [49], and even though the conductivity at high temperature was similar to the one in Ref. [61],

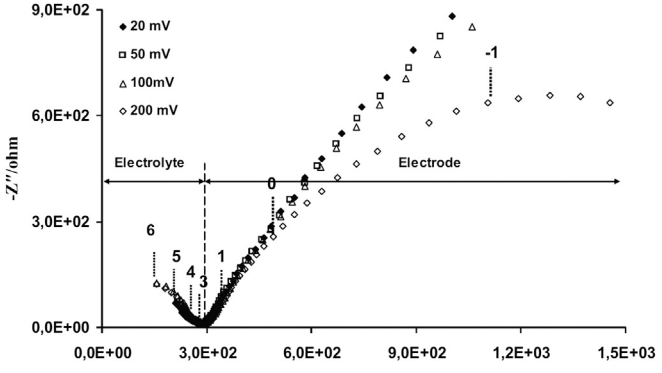

Fig. 2. Impedance measurements below the melting point of the carbonate mixture using different amplitudes. Reproduced from Ref. [16] with permission from Elsevier, Copyright 2011.

there was also a leap in the conductivity around 400 °C (most likely due to different sintering conditions in the articles). In both of the articles the high conductivities were attributed to the co-doping and the enhanced conduction through the interfaces between the oxide and carbonate. The conductivities were still high compared to other composites with similar structures, so most likely there are still other (unknown) reasons for the high performance.

4.2.2. The effect of the carbonates

In most of the articles studied, the slope in the Arrhenius plot changed around a certain temperature, which was around, and often even below, the melting point of the carbonate mixture. In many cases a (nonlinear) leap in the conductivity around that temperature point was observed. However, in several of the papers, the reported conductivity was practically linear throughout the measurement range with a possible change in the slope around the melting point [14,49,60–64]. The conductivity could also increase in several smaller steps below the melting point of the eutectic Li/Na carbonate mixture after which the conductivity would again be linear [53]. Additionally, the structure and the size of the composite particles may affect the conductivity as a leap in conductivity could have appeared even below 400 °C for doped ceria/sodium carbonate composites [13,49] even though the melting point of the sodium carbonate is 851 °C [65].

The EIS measurements have mostly been performed by working from low temperature to high temperature but in Ref. [51] the conductivity was also measured when the temperature was decreased back to the starting temperature. Additionally, at least 30 min was waited between the measurement points to decrease the errors of having a nonhomogeneous or incorrect temperature in the sample. During the heating, a leap in the conductivity appeared around 490 °C after which the conductivity was linear. However, during the cooling cycle the conductivity did not drop rapidly until around 450 °C. Similarly, in the differential scanning calorimetry (DSC) measurements the composite showed a peak at 483 °C during heating and at 440 °C during cooling. Additionally, the rapid increase in conductivity of a pure carbonate mixture occurred

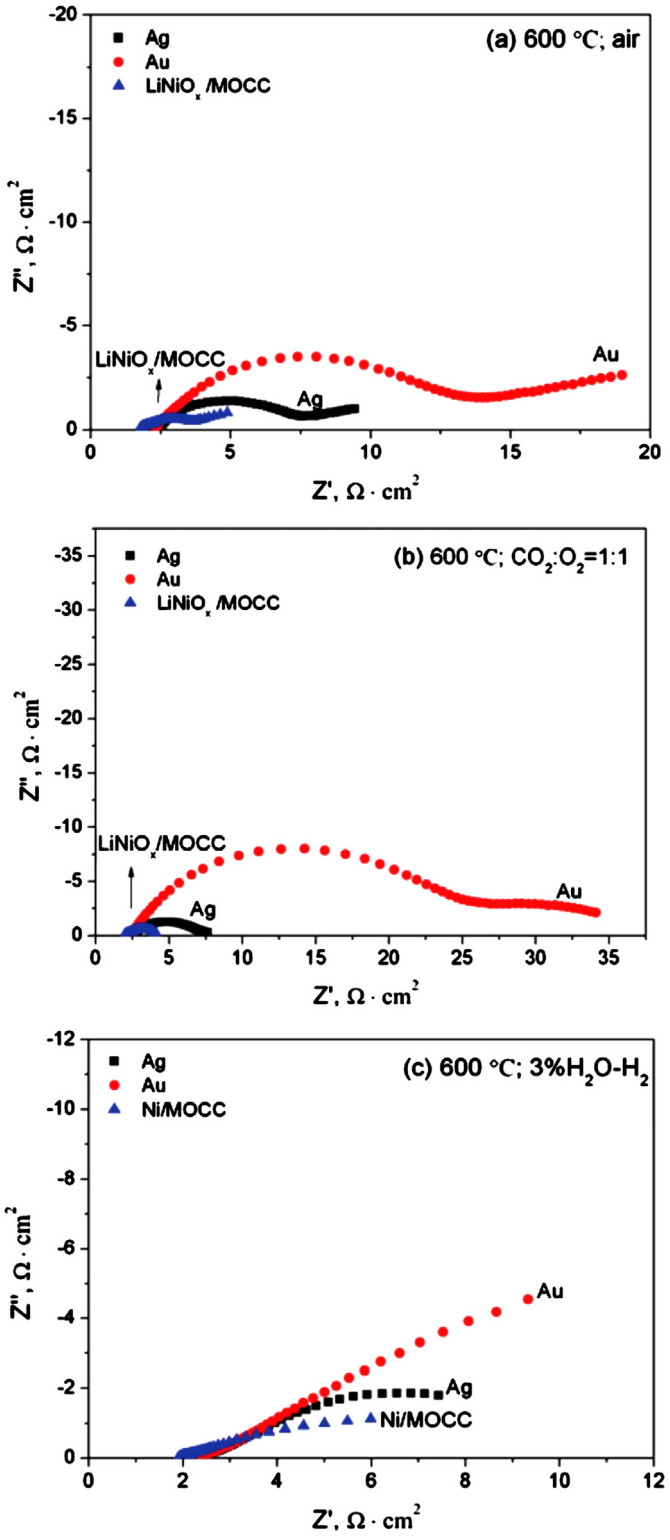

Fig. 3. AC impedance spectra of GDC/(Li,K)CO_3 composites measured at 600 °C with different electrodes and various atmospheres: a) air; b) CO_2:O_2 = 1:1; c) 3% H_2O–H_2. The difference in ohmic resistance (high frequency intersection with Z′ axis) is caused by different sample thicknesses. Reproduced from Ref. [51] by permission of ECS, The Electrochemical Society, Copyright 2011.

around 470 and 490 °C. These results would imply that the carbonate could stay molten even at temperatures below the melting point and that the increase in the conductivity would mainly be due to the softening of the carbonate mixture.

Generally the conductivity of the doped ceria/carbonate composite increased with the carbonate content at temperatures above the melting point, while the opposite applied at low temperatures. This is because the conductivity of solid carbonates is lower than that of the doped ceria while molten carbonates have higher conductivity [51] and below the percolation threshold the carbonate particles may be separated by SDC particles thus blocking transportation of carbonate ions [66]. However, in some of the measurements where the conductivities of a composite and pure doped ceria were measured, the conductivity of the composite is higher than that of the doped ceria even at low temperatures [3,61,67]. As a side note, no real consensus has been found on how the ratio between doped ceria and carbonate affects the melting point of the composite [14,16,17,21,48].

The effect of having different mixtures of carbonates has been investigated in Refs. [15,67] where $Ce_{0.8}Sm_{0.2}O_{1.9}$ was mixed with $(Li,Na)_2CO_3$, $(Li,K)_2CO_3$ and $(Na,K)_2CO_3$ (the ratio of alkali metals was around 1:1). Both impedance and *I–V* measurements were performed on the samples and assorted data are shown in Fig. 4. The impedance conductivity (in air) of the (Na,K) sample was more than an order of magnitude lower than the conductivity of the other samples. However, the values of the power densities at 600 °C and the conductivity from the *I–V* measurements were much closer to each other. Additionally, conductivity and fuel cell measurements were performed in Refs. [21,48] for samples with varying carbonate contents. The conductivity (in air) increased practically with the carbonate content while the best power densities over the melting temperature were achieved with samples with an average carbonate content (20 wt% to 30 wt% of carbonates). These observations would imply that the conductivity values obtained from the impedance measurements cannot be used as such when comparing the properties of the electrolyte in an operating fuel cell and that there is a ratio of doped ceria to carbonate where the conductivity through the interfaces is optimized for fuel cell operation.

The influence of the carbonate mixture has also been studied using other oxide/carbonate composites besides doped ceria. In Ref. [17] the conductivity of alumina:LNC ($(Li_{0.67}Na_{0.33})_2CO_3$) and GDC:LNC samples with various carbonate contents were studied. The conductivities of alumina:LNC samples with 35 and 40 wt% of LNC were on par with GDC:LNC samples with the same carbonate content at temperatures over the melting point. However, with lower carbonate contents the conductivity of GDC:LNC was at least an order of magnitude higher. Interestingly, the linear part of the conductivity curve (after the rapid increase) appeared at around 500 °C for the alumina:LNC samples with 35 and 40 wt% carbonate contents, while for lower contents the increase in the conductivity did not appear before 600 °C. In Ref. [56] the conductivity of pure alumina, yttria-doped tetragonal polycrystalline zirconia (TZP), ceria and SDC as well as composites with 50 vol% of $(Li_{0.33}Na_{0.67})_2CO_3$ and pure carbonate were studied. There was no rapid increase in conductivity with alumina composite but with the other composites the leap occurred around 475 °C–525 °C. Also the conductivities of the composites were higher than those of pure materials except for the pure carbonate whose conductivity was the highest of them all over the melting point of the carbonate. Of the composites, the ceria composite showed the best conductivity in this temperature range even though the conductivity of pure ceria is less than that of the SDC. However, the ceria particles were in this case significantly smaller than the SDC particles. The size of the particles could in principle both ease the developing of the continuous carbonate structure as well as increase the interface area between the oxide and carbonate layers.

The effect of the macroscopically continuous SDC and carbonate structures has also been studied [11,12,57]. In Ref. [11] a porous SDC structure was prepared by a sacrificial method by removing NiO

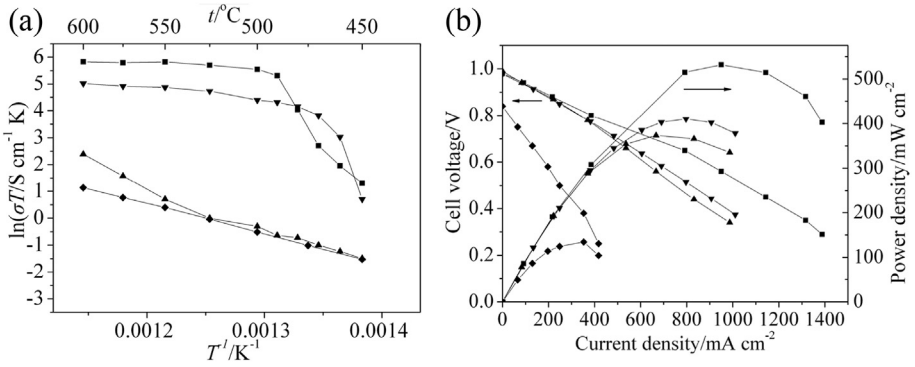

Fig. 4. a) Temperature dependence of conductivity for SDC-carbonate composites and SDC and b) *I*–*V* and *I*–*P* characteristics of fuel cells at 600 °C: (■) SDC with $(Li,Na)_2CO_3$; (▼) SDC with $(Li,K)_2CO_3$; (▲) SDC with $(Na,K)_2CO_3$; (◆) SDC. Reproduced from Ref. [67] with permission from The Trans Tech Publications, Copyright 2010.

from the prepared cell. The structure was then immersed into a molten $(Li,Na)_2CO_3$ mixture, which produced continuous SDC and carbonate structures with a micrometer scale thicknesses. Even though the SDC phase was in the micrometer scale, a high conductivity value was achieved beyond the melting point. The conductivity also increased at temperatures above the melting point as the amount of the carbonate was increased. However, the conductivity with CO_2/O_2 (1:1) gas was lower than with wet H_2 and air, which opposes the understanding of the major contribution of carbonate ions on the total conductivity. In Ref. [12] both molten salt infiltration and "conventional mixing-pressing" methods were used. Higher conductivities were reported for the sample made by the molten salt infiltration method owing to the continuous SDC structure although also the carbonate structure could have caused the better results. The effect of the continuous structure was also studied in Ref. [57] where multilayer, homogeneous and single layer cells where prepared. In the multilayer cells $Ce_{0.9}Gd_{0.1}O_{1.95}$ (GDC) and $(Li_{0.33}Na_{0.67})_2CO_3$ (LNC) layers alternated, in the homogeneous cells the materials were mixed together and in single layer cells either pure LNC or GDC was used. The conductivity of the multilayer cells was measured both in series and in parallel configurations. It was noted that the parallel configuration yielded similar values than pure GDC while the series configuration yielded similar behavior as the LNC cell (conductivity of LNC cell was higher than that of pure GDC at temperatures over around 450 °C and lower below that). They concluded that apparently the ceramic/salt interface did not show significant contribution on the conductivity. However, it should be mentioned that in the homogeneous samples the actual interface area is practically much larger than with multilayer cells and the preparation of the interfaces is different in these cases, so the results for the multilayer cell might not be directly extrapolated to function with homogeneous cells. Nevertheless, according to these results it seems that the continuous carbonate/SDC structure can enhance the total conductivity, but it is not clear how good performance the cells would show in fuel cells. Also preparing thin electrolytes for the fuel cells with the molten salt infiltration or other similar methods might be challenging.

Combining these observations, it seems likely that the conductivity of the ions in the carbonate melt attributed mostly to the total conductivity over the melting temperature of the carbonates. However, it has also been proposed that a space charge zone appears on the interface between the doped ceria and the (partially molten) carbonate thus increasing the total conductivity by generating a "superionic pathway" for the ions [17,52,58,68]. Unfortunately, it is hard to distinguish the different conduction mechanisms and transport numbers with EIS only so other methods are needed to define the relative effect of the ions.

5. Constant current measurements

5.1. Theoretical fundamentals

In the constant current method, an external constant current is conducted through the sample. At first, the ions in the sample move according to the direction of the current until a steady state is achieved. Under this static state, only electrons and externally supplied ions corresponding to the gas atmospheres continue to move assuming that the sample does not deteriorate, e.g. carbonate ions do not transform into carbon (di)oxide and oxygen molecules. Finally the specific ion conductivity can be defined from the voltage and current values assuming that the electronic conduction as well as other voltage polarizations can be determined or are negligible. One can supply the gas atmosphere using a single chamber where there are no distinct anode and cathode atmospheres, but generally the gases are supplied separately on both sides of the sample. If the concentration (or more specifically the activity) of the gas molecules is different on either side of the sample, a concentration polarization is generated according to Nernst equation [2]. In this section we are concerned only about measurements with similar gas atmospheres on both sides of the cell, and the measurements with different gas atmospheres are shown later under Section 6.

Typically either 2 or 4-point method is used in the conductivity measurements. The polarizations due to the electrodes can be neglected in the 4-point method, but the positions of the four wires as well as the contact area between the wires and the sample are important as these affect the potential distribution. This can cause artifacts to the results unless these effects are taken into account. Examples of how the position of the wires affects the potential distribution are illustrated through two simple simulations that are shown in Fig. 5. The simulations were performed with COMSOL Multiphysics program with the following specifications: conduction is assumed to be isotropic in the sample, a constant current (density) is supplied to one current probe and the same current exits through the other current probe, and all the other parts are electrically insulated. For example, in the case of a rotationally symmetric sample, where the current probes are attached on the outer part of the sample and the voltage probes on the axis, clearly too small potential difference (higher conductivity) would be attained if corrections for the potential distribution are not made. More information about correcting errors and assembling a 3 or 4-point measurement system can be found in Refs. [45,59,69,70].

5.2. Results

Specifically chosen data of recent constant current measurements of the doped ceria/carbonate composites are shown in

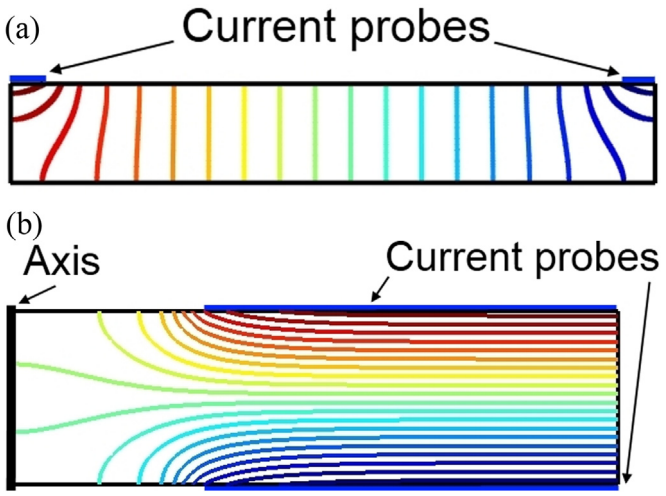

Fig. 5. Voltage distributions in the sample with different probe placements. Constant current densities (negative and positive) were applied through the electrodes while the other parts were electrically insulated. (a) A two dimensional bar and (b) a rotationally symmetric sample (a cylinder).

Table 5. The effect of using different electrodes is illustrated in Ref. [71] where the electrolyte conductivity was measured with the 2-point method using two different electrode complexes with a constant current of 0.1 A. The sample configurations were the following: "Ag (paste)/electrolyte/Ag (paste)" and "Ag (paste)/mixed electrode/electrolyte/mixed electrode/Ag (paste)", where the mixed electrode was either electrolyte + NiO (in H_2 atmosphere) or electrolyte + lithiated NiO (in oxidative atmosphere). As the conductivities with mixed electrode layers were higher than without them, it seems that the electrode contributions were not taken into account when ion conductivities were calculated. For this reason the conductivities given in the table should most likely be even higher for the corresponding article. In fact, the conductivity was also determined from the I–V curve and it was 2.5–3 times the sum of the 2-point conductivities in air and hydrogen. Nevertheless, this shows that the electrode contribution can be significant and should be taken into account even if good catalysts are used at high temperatures.

Two different 4-point attachments have been explained in the reviewed articles. In the first one, a platinum ring (a current probe) and a point inside it (a potential probe) were painted on both sides of a round pellet according to Fig. 6a [58,72,73]. According to the

Table 5
Summary of the constant current measurements.

Materials				Measurement				Conductivity					Power dens.		Ref.
Oxide		M_2CO_3 (mol%)		Method	Electrode		Gases	Max S cm^{-1}	T °C	@550 °C S cm^{-1}	Slope change	Temp. range	Max mW cm^{-2}	T °C	
Formula	Amount	Li	Na		Mat.	Form									
$Ce_{0.8}Sm_{0.2}O_{1.9}$	100 wt	52	48	4-probe	Ag	Bar	Air	7.5e-3	650	2.7e-3	No	425–650			[74]
	90 wt	52	48	4-probe	Ag	Bar	Air	1.0e-2	650	3.3e-3	500	425–650			
	80 wt	52	48	4-probe	Ag	Bar	Air	2.0e-2	650	6.3e-3	500	425–650			
	70 wt	52	48	4-probe	Ag	Bar	Air	2.9e-2	650	1.1e-2	500	425–650			
	60 wt	52	48	4-probe	Ag	Bar	Air	3.9e-2	650	1.3e-2	500	425–650			
	0 wt	52	48	4-probe	Ag	Bar	Air	6.6e-2	650	2.6e-2	500	425–650			
	90 wt	52	48	4-probe	Ag	Bar	H_2	2.1e-3	650	3.9e-4	No	425–650			
	80 wt	52	48	4-probe	Ag	Bar	H_2	5.0e-3	650	9.7e-4	No	425–650			
	70 wt	52	48	4-probe	Ag	Bar	H_2	1.3e-2	650	2.9e-3	No	425–650			
	60 wt	52	48	4-probe	Ag	Bar	H_2	2.0e-2	650	4.2e-3	No	425–650			
	0 wt	52	48	4-probe	Ag	Bar	H_2	3.9e-2	650	7.2e-3	No	425–650			
$Ce_{0.8}Sm_{0.1}Nd_{0.1}O_{1.9}$	100 wt	66.7	33.3	4-probe	n/a	n/a	Air	1.5e-2	700	4.0e-3	No	350–700			[75]
	90 wt	66.7	33.3	4-probe	n/a	n/a	Air	3.3e-2	700	1.0e-2	550	350–700			
	80 wt	66.7	33.3	4-probe	n/a	n/a	Air	1.9e-1	700	5.5e-2	490	350–700			
	70 wt	66.7	33.3	4-probe	n/a	n/a	Air	1.2e-1	700	2.5e-2	550	350–700			
	60 wt	66.7	33.3	4-probe	n/a	n/a	Air	3.2e-2	700	1.9e-2	490	350–700			
$Ce_{0.8}Sm_{0.2}O_{1.9}$	80 wt		100	4-probe	Pt	Ring	5% H_2[c]	6.0e-2	600	5.1e-2	350	200–600			[72]
	80 wt		100	4-probe	Pt	Ring	21% O_2[c]	4.9e-3	600	3.1e-3	No	200–600			
	80 wt		100	WH[a]	Pt	n/a	n/a	3.0e-4	600	2.0e-4	n/a	550 & 600			
$Ce_{0.8}Ca_{0.2}O_{2-\delta}$	80 wt		100	4-probe	Pt	Ring	5% H_2[c]	5.2e-2	600	4.3e-2	400	200–600			[58]
	80 wt		100	4-probe	Pt	Ring	Air	4.5e-3	600	2.5e-3	No	200–600			
$Ce_{0.8}Sm_{0.2}O_{1.9}$	95 wt		100	4-probe	Pt	Ring	5% H_2[c]	6.0e-2	650	4.3e-2	350	200–600	514[d]	550	[73]
	90 wt		100	4-probe	Pt	Ring	5% H_2[c]	8.0e-2	650	6.3e-2	350	200–600	833[d]	550	
	85 wt		100	4-probe	Pt	Ring	5% H_2[c]	7.0e-2	650	5.7e-2	350	200–600	729[d]	550	
	80 wt		100	4-probe	Pt	Ring	5% H_2[c]	6.3e-2	650	4.7e-2	350	200–600	613[d]	550	
	95 wt		100	4-probe	Pt	Ring	21% O_2[c]	8.0e-3	650	3.7e-3	No	200–600			
	90 wt		100	4-probe	Pt	Ring	21% O_2[c]	7.0e-3	650	3.7e-3	No	200–600			
	85 wt		100	4-probe	Pt	Ring	21% O_2[c]	8.0e-3	650	3.3e-3	No	200–600			
	80 wt		100	4-probe	Pt	Ring	21% O_2[c]	7.0e-3	650	3.0e-3	No	200–600			
$Ce_{0.8}Sm_{0.2}O_{1.9}$	80 wt	66.7	33.3	2-probe	Elec.[b]	Pellet	Air			1.8e-2	n/a	450 & 550			[71]
	80 wt	66.7	33.3	2-probe	Elec.[b]	Pellet	H_2			4.0e-2	n/a	450 & 550			
	80 wt	66.7	33.3	2-probe	Ag	Pellet	Air			1.7e-2	n/a	450 & 550			
	80 wt	66.7	33.3	2-probe	Ag	Pellet	H_2			3.8e-2	n/a	450 & 550			
	80 wt	66.7	33.3	IV	Ag	Pellet	Wet H_2/air			1.5e-1	n/a	550	780[e]	550	
CeO_2	100 wt			2-probe	Ag	Bar	Air	1.0e-3	900	1.2e-6	No	450–900			[87]
	80 wt		100	2-probe	Ag	Bar	Air	1.6e-3	650	3.4e-4	No	200–650			

[a] WH = Wagner–Hebb (electronic conductivity) measurement, where Pt paste and foil were used as reversible electrode and blocking electrode, respectively.
[b] Electrodes consisted of a mixed electrode (Ni or lithiated NiO + SDC-carbonate) and Ag paste.
[c] % sign implies that the rest of the gas is N_2.
[d] H_2/synthetic air.
[e] Wet H_2/air.

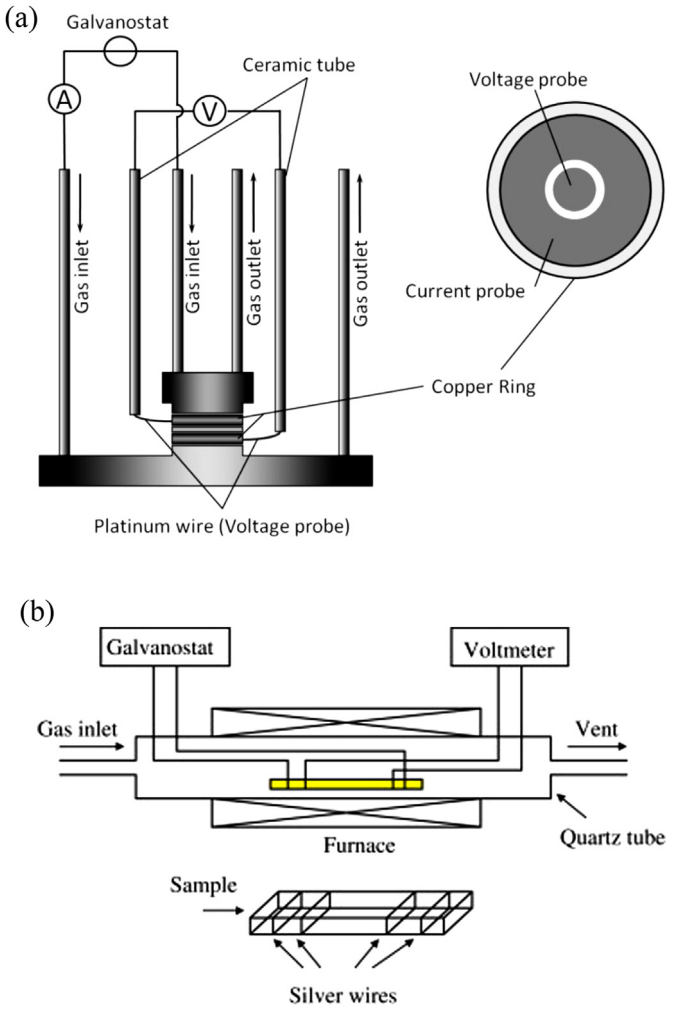

Fig. 6. (a) The schematic diagram of the 4-point DC current measurements with a cylinder-like construction. Reproduced from Ref. [88] with permission from the author, Copyright 2012. (b) The schematic diagram of the 4-point DC current measurements with a bar-like construction. Reproduced from Ref. [74] with permission from International association for hydrogen energy, Copyright 2013.

discussion about the simulation and as no information about the voltage correction was given, in reality the conductivities might be lower. In the second one, the electrolyte was made into a bar and silver wires were attached on top of it (the current wires near the edges and the potential wires between the current wires) as is shown in Fig. 6b [74]. A 4-point method was additionally used in Ref. [75] but unfortunately there was no information about how the wires were attached.

In most of the constant current measurements, the conductivities in oxygen and hydrogen rich atmospheres were compared with each other. In Ref. [71] σ_{H^+} was 2–3 times higher than $\sigma_{O^{2-}}$ but as the electrode contributions were most probably not taken into account in the 2-point method, the exact difference remains unclear. In Ref. [74] a 4-point method was used to measure the conductivities and $\sigma_{O^{2-}}$ was higher than σ_{H^+}. The difference was at highest with low carbonate contents but decreased as the carbonate to oxide ratio increased. Additionally, there was a distinct leap in $\sigma_{O^{2-}}$ at around 500 °C (melting temperature of the eutectic $(Li,Na)_2CO_3$ composition) while σ_{H^+} was only slightly enhanced around the same temperature. On the other hand, in other 4-point measurements the σ_{H^+} was about an order of magnitude higher than $\sigma_{O^{2-}}$ at temperatures above the melting point [58,72,73]. Even though no corrections due to the positions of the probes were done, it should not have affected the relative conductivities largely. Additionally, only σ_{H^+} exhibited a rapid increase and the leap appeared at 350 °C–400 °C, far below the melting point of the sodium carbonate. Unless the increase at so low temperature could be attributed to an increased electronic conductivity due to hydrogen atmosphere, the previous results would imply that the preparation methods greatly affect whether oxygen ion or proton conductivity is higher.

In fact the electronic conductivity was additionally measured in Ref. [72] using a Wagner–Hebb measurement (more information of the method can be found in Refs. [76,77]). The method in Ref. [72] is based on blocking the ion conduction with a Pt foil (a blocking electrode) while Pt paste was used on the other side of the cell (a reversible electrode). Unfortunately, there was no mentioning about what kind of atmosphere was used on the reversible electrode i.e. it was not mentioned if, for example, a low p_{O_2} would have caused higher electronic conductivity. In addition, it is possible that the ion movement cannot be completely blocked, i.e. the actual electronic conductivity would be lower than the measured one [75]. Nevertheless, the measured σ_{e^-} was one order of magnitude lower than $\sigma_{O^{2-}}$ and 2 orders of magnitude lower than σ_{H^+}. The electronic conductivity is generally assumed insignificant but the aforementioned electronic conductivity may in fact have a significant contribution to the conductivity. Thus more research should be focused on the electronic conductivity of the LT-SOFC composite electrolyte.

Similarly to the results of the EIS measurements, the effect of the carbonates cannot be easily generalized. In Refs. [73,75] the conductivities do not follow any simple rule, but in Ref. [74] both proton and oxygen ion conductivities of the composite increased with the carbonate content, when the temperature was above the melting point (around 500 °C) and decreased below that temperature. Additionally, the conductivity of the pure carbonate was also measured in Ref. [74], and it had the highest conductivity of the samples over the melting point of the carbonate mixture. However, the transport mechanisms in the pure carbonate are not clear. Protons could in principle be transported in HCO_3^- ions without affecting the stability of the carbonate. However, with oxygen ion conductivity the following (or similar) reaction would most likely take place on the electrodes:

$$CO_3^{2-} \rightleftharpoons CO_2 + O^{2-} \quad (3)$$

Thus the high conductivity in air would mean that: a) the electronic conductivity is high, b) the carbonate deteriorates over time if there is not enough carbon dioxide in the air or c) there are other conductivity methods. The electronic conductivity was indeed measured and deducted from the conductivities using the Hebb–Wagner measurement, and it was simply mentioned to be much lower than the measured conductivities. Unfortunately, the effect of b) and c) is not clear with the current data so further experiments are needed to deduce the reason for the high conductivity of pure carbonate in air.

In summary, the pros of the constant current measurement include the possibility to separate the ionic conductivities and possibly also the electronic conductivity from each other. However, the cons incur that the measurement has to be performed in a specific atmosphere where the desired ions can move, i.e. the conductivities in true fuel cell operating conditions might differ slightly from the ones that were measured. Additionally, with the 4-point method (that is not only limited to the constant current measurements, though) it is also possible to remove the effects of the electrodes but care has to be taken that the errors

corresponding e.g. to the potential distribution and electrode reactions can be excluded.

6. Product analysis measurement

The main idea of the product analysis measurement is the following: Assuming that the electronic conductivity is negligible in the electrolyte, the current in the electrolyte is due to the movement of the ions. The total conductivity can be measured if the voltage and the current through the electrolyte is known. The relative conductivities of the ions can then be measured by comparing the amount of molecules that pass through the cell, i.e. the transport numbers. Similarly to the constant current measurements, the voltage loss related purely to the electrolyte has to be measured in a separate measurement, with a 4-point method or in several 2-point measurements. Unfortunately, as the gas atmospheres have to be separate on anode and cathode sides and the gases have to be monitored and controlled carefully, this restricts the possible configurations for the 4-point method. However, if the measurement is done correctly, it is possible to measure the specific ionic conductivity of several species simultaneously.

Product analysis methods were used to measure the ionic conductivities in Refs. [78,79]. In Ref. [78] H_2 was supplied to one side and either O_2, or O_2 and CO_2 (1:1) to the other side. Incoming gas flows, produced water as well as CO_2 gas flow on the anode side were measured. In Ref. [79] active gas (H_2 or O_2) was supplied to one side and argon to the other side and the gas flow of the active gas was monitored on both sides. One of the biggest difficulty with the product analysis method is the exact measurement of the mass flows. In addition to the inaccuracies due to the mass flow monitors, the measurement system and the sample are also never absolutely gas tight, i.e. there are always gas leakages. In Refs. [78,79], the effect of the leakages was determined by first measuring the gas flows at OCV and then deducting this value from the gas flows when current was supplied over the sample. However, the leakage might decrease when current is supplied [80] so the measured amount that is going through the sample may be actually slightly larger. Nevertheless, at high current densities the leakage through the cell should be insignificant compared to the ionically conducted species [80] and leakage through the edges should stay mostly constant.

The voltage over the electrolyte was measured with a current interruption method in Refs. [78,79]. In this method, a constant current is first applied through the sample after which the current is abruptly cut to zero. This causes the voltage to change in time and enables the determination of ohmic (fast) and non-ohmic (slow) effects. However, the time between two voltage points has to be small in order to get accurate results. More information about the current interruption method can be found in Ref. [81]. In Ref. [79] a constant 100 mA current was applied through the cell in a charging mode (voltage higher than OCV) and then interrupted. An abrupt decrease of voltage was detected within 10 μs after which the voltage decreased slowly to OCV. The whole sudden change was attributed to the resistance of the electrolyte as the ohmic losses on the platinum electrodes were assumed insignificant. The slow decrease was then attributed to electrode reactions. However, it was not defined whether the resistance of the wires and contacts was taken into account. This could have been done for example by using 4 wires or by measuring the effect of the wires separately. Unfortunately, in Ref. [79] no specific information on the measurement data was given. Additionally, according to earlier impedance measurements, the time constants of ionic conductivities (bulk and grain boundary) are assumed to be close to each other, and at high temperatures time constant of less than 10 μs have been acquired in most of the impedance measurements. This supports that current interruption method could be used for measuring the electrolyte resistance assuming that the measurement device can record quick changes and other ohmic resistances are insignificant compared to the electrolyte resistance. Unfortunately, this is not always true.

Most of the measurements were performed at 650 °C and the data of those are presented in Table 6. The conductivities increase as the carbonate content is increased. This was expected from $\sigma_{CO_3^{2-}}$ but happens also for σ_{H^+} and $\sigma_{O^{2-}}$. Additionally, when CO_2 was supplied, the total conductivity increased while $\sigma_{O^{2-}}$ decreased. σ_{H^+} remained practically constant (still lower than $\sigma_{O^{2-}}$) when CO_2 was supplied [78]. When compared to other measurement methods, the conductivities acquired with the product analysis method were mostly lower than with EIS, but similar values were acquired with the constant current methods. This is not surprising as the conductivities of other ion species are not easily deducted from the total conductivity in EIS measurement. It can also be noted that the product analysis method can be thought to be an improved version of the constant current measurements but its largest disadvantage is the need for the accurate measurement of the gas flows. However, if the voltage over the electrolyte and the mass flows can be measured/controlled accurately, several conductivities can be measured at the same time and during the operating fuel cell conditions.

7. Overview of the characterization methods and measurement configurations, and recommendations for future studies

As shown in the previous sections, different techniques have been used for measuring the (ionic) conductivity of doped ceria/

Table 6
Summary of the product analysis measurements.

Materials				Conductivity at 650 °C (S cm^{-1})					Ref.
Oxide		M_2CO_3 (mol%)		Gases	H^+	O^{2-}	CO_3^{2-}	Total	
Formula	Amount	Li	Na						
$Ce_{0.8}Sm_{0.2}O_{1.9}$	90 wt	52	48	H_2/O_2	4.0e-3	1.7e-2		2.1e-2	[78]
	90 wt	52	48	$H_2/O_2 + CO_2$	5.0e-3	7.7e-3	1.6e-2	2.9e-2	
	80 wt	52	48	H_2/O_2	1.2e-2	3.5e-2		4.7e-2	
	80 wt	52	48	$H_2/O_2 + CO_2$	1.2e-2	2.6e-2	3.8e-2	7.6e-2	
	70 wt	52	48	H_2/O_2	1.6e-2	5.2e-2		6.8e-2	
	70 wt	52	48	$H_2/O_2 + CO_2$	1.5e-2	3.3e-2	5.3e-2	1.0e-1	
$Ce_{0.8}Sm_{0.2}O_{1.9}$	95 wt	52	48	Gas/argon[a]	6.0e-3	1.5e-2		2.1e-2	[79]
	90 wt	52	48	Gas/argon[a]	1.0e-2	2.1e-2		3.1e-2	
	80 wt	52	48	Gas/argon[a]	1.8e-2	5.5e-2		7.3e-2	
	70 wt	52	48	Gas/argon[a]	2.2e-2	7.1e-2		9.3e-2	

[a] Argon was supplied to the other side and either H_2 or O_2 to the other side of the cell.

carbonate composite electrolyte. Unfortunately, it seems that not all of the measurements reported have been properly conducted and all of the methods are not even valid for such measurements. For this reason each method and their suitability is briefly illustrated. Also as the electronic conductivity needs to be excluded to evaluate the ionic property of the composite electrolyte, we will briefly introduce a few possible electronic conductivity measurement techniques as well. Following this, we will also elaborate on the electrode configurations and stability issues as these affect the measurement accuracy and should always be taken into account. Finally, we will recommend several approaches that can be used to acquire more accurate data.

7.1. Electrochemical impedance spectroscopy

Electrochemical impedance spectroscopy (EIS) is currently the most commonly used method for measuring the conductivity of doped ceria/carbonate composite electrolytes. Unfortunately, it is practically impossible to differentiate the effects between the different conduction pathways due to overlapping time constants (semicircles). Therefore, only the total conductivity that includes all the ion conductivities can be determined. However, this leads to a too high conductivity value compared to the actual effective conductivity of the electrolyte during real fuel cell operation. Thus EIS may not be well suitable for measuring the conductivity of (nano) composite samples.

7.2. Constant current method

The constant current method gives conductivity values that reflect the effective conductivity of the electrolyte in an operating fuel cell. This is because only the specific ions associated with the prevailing atmosphere (and electrons) can contribute to the overall charge transportation. The conductivity can be measured both in 2-point and 4-point measurements. However, unless several samples of different thickness are used in the 2-point measurements, no accurate values can be attained with this method as it is hard to distinguish the electrolyte contributions from other components in the data. In the 4-point measurement, accurate results are obtained only if the electrodes are positioned in specific well-known geometries, or if the potential distribution with the specific wire configuration is modeled and the measured results are corrected accordingly. Unfortunately, such corrections were seldom found in the reviewed articles. Additionally, the electronic conductivity should be measured separately and deducted from the total conductivity in order to obtain the ionic conductivity. Nevertheless, if the constant current method is applied correctly, accurate specific ion conductivity values can be obtained.

7.3. Product analysis method

With the product analysis method it is possible to measure several conductivities (including electronic conductivity) simultaneously. However, the method yields reliable data only if mass flow rates can be measured exactly, i.e. the sample is well sealed and mass flow controllers and meters are accurate, which leads to a limited number of choices of possible wiring geometries compared to the constant current method. The electrode contributions have to be also taken into consideration in the same way as in the constant current method. In the reviewed articles, the voltage was measured with the current interruption method, but a 4-point measurement configuration could give more accurate results. Similar gas atmospheres as in an operating fuel cell (hydrogen on the anode and oxygen and carbon dioxide rich gases on the cathode) could be used to obtain more realistic conductivity values.

7.4. Electronic conductivity measurements

The electronic conductivity was measured in the reviewed articles using a 2-point Hebb–Wagner method where only one side of the sample is exposed to gas and the other side is in contact with metal. The idea is that only electrons would be able to conduct through the sample when a constant current is driven through the sample. Unfortunately, even though the gas atmospheres influence the properties of the sample, no detailed information on gas atmospheres were mentioned in any of the reviewed articles. Additionally, a 2-point measurement is valid only under some restrictive conditions and a 4-point configuration is highly recommended in order to detect if the restrictions truly apply in the measurement [77]. Even though an ion blocking electrode is used on the other side of the sample, ions may still move in it, for example, due to insufficient sealing and if the moving ions have different valence states [77]. However, though accurate electronic conductivity values may not always be obtained, a low (total) conductivity will also indicate a low electronic conductivity. Summarizing, until more experience from the Hebb–Wagner method for the doped ceria/carbonate composite samples is available, one should consider reported values as indicative only.

In addition to the Hebb–Wagner method, the electronic conductivity could in certain situations be measured with the constant current and product analysis methods. In the constant current method a non-active gas (e.g. N_2) is fed to the sample and theoretically only electrons should be able to transport through the sample. However, the electronic conductivity value would be indicative only as the oxidative and reducing gas atmospheres in a fuel cell can affect the properties of the sample. In the product analysis method, the movement of the ions through the sample can be determined by measuring the mass flows on both sides of the sample. As the total current is composed of the movement of both ions and electrons, one can calculate the relative conductivities from these currents if mass flow rates are measured accurately. All of above methods may suffer from stability issues of the sample, but if performed correctly, the methods can provide at least indicative values for the electronic conductivity.

7.5. Electrode configurations

The 2-point measurement is the most commonly used configuration, especially in the EIS measurements. In the EIS it is possible to distinguish the effects of electrode and electrolyte contributions from each other but in the constant current and product analysis methods this is not possible with a single measurement. However, this problem can be circumvented by measuring the resistance of several samples with different electrolyte thicknesses and then calculating the electrolyte conductivity from these results. This could be a relatively accurate and a rather simple method assuming that around 5 or more samples are measured per each electrolyte. Unfortunately, this requires large material amounts and is also time consuming.

In the 4-point measurements different wiring configurations, e.g. bar and coin geometries (Fig. 7a and c) have been utilized so far. The results in the coin geometry need to be corrected according to potential distribution models. On the other hand, in the bar geometry, the potential difference is practically linear with respect to the distance between the probes if the potential probes are sufficiently far away from the current probes and the potential probes are much smaller than the distance between the probes. Similarly to the bar geometry, instead of having the voltage probes on the edge of the sample, the voltage probes can also be inserted in a so-called Luggin probe geometry, where small holes are drilled in the middle of the sample as shown in Fig 7b [59]. This geometry allows

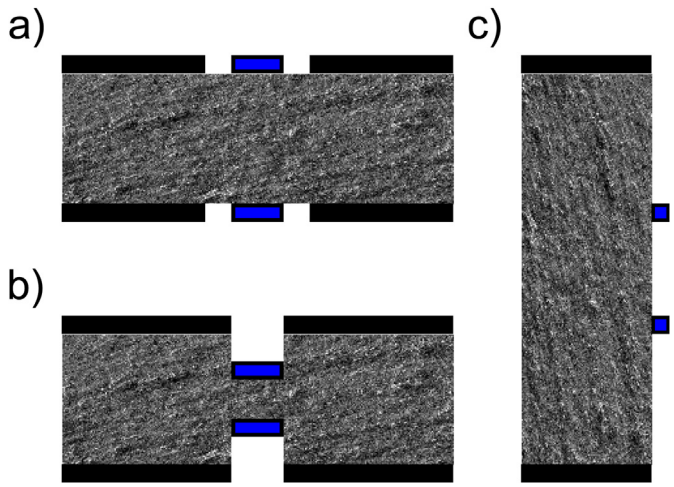

Fig. 7. Schematic diagrams of several different 4-point electrode geometries: (a) coin, (b) Luggin probe and (c) bar. Blue and black parts represent voltage and current probes, respectively. The thicknesses of the probes are greatly exaggerated. (For interpretation of the references to color in this figure legend, the reader is referred to the web version of this article.)

sealing of the sample edges and using different atmospheres on both sides of the sample. However, sample preparation is more difficult compared to the other configurations. Naturally it is also possible to use other geometries as well as long as the potential distribution is modeled and taken into account in the results.

The van der Pauw configuration has been used for measuring (electron and hole) conductivities in semiconductor materials [82], but could also be suitable for composite materials. In this method four probes are inserted on the same side of a thin and wide sample. The current and the voltage between the probes are then measured in several different combinations and a specific equation is used to estimate the conductivity of the sample [82]. As this method has not been used with the composite materials yet, its accuracy is still unknown.

In conclusion, a 2-point configuration is easier to implement, but it needs several measurements to be accurate while a 4-point configuration needs only one measurement, but the potential distribution has to be modeled for the particular geometry. Nevertheless, it is always recommended to use short, shielded cables, if possible, and assure that the contact between the sample and the wires is as smooth as possible.

7.6. Stability issues

Gas atmospheres in particular can cause large stability problems. Hydrogen, for example, can lead to higher electronic conductivity due to the reduction of doped ceria at higher temperatures. Additionally, when one measures the conductivity of "extrinsic ions", these have not yet reached the other side of the sample at the beginning of the measurement. However, the redox reactions take place on both electrodes simultaneously indicating that there are other (undesired) reactions occurring on the other electrode. The ions from these reactions can cause both stability issues and extra ion transportation. However, if wet gases are used, it is possible that hydroxyl ions and hydrogen are produced instead, thus preserving the sample but adding a new ion that will contribute to the total conductivity. Additionally, even after a stable flow of the "extrinsic ions" through the electrolyte has been reached, the extra ions from other reactions can still contribute to the total conductivity.

In addition, high applied potentials bring similar complications as the "extrinsic atmospheres" due to undesired reactions. High potentials should therefore be avoided and measurements should start with determining the conductivity in "intrinsic atmospheres", then moving to "extrinsic atmospheres" and finally measure the conductivity again in "intrinsic atmospheres" in order to validate the stability of the sample during the measurement. If the results differ greatly from each other, that particular measurement method should not be used for measuring the "extrinsic ion" conductivity. The product analysis method with similar gas atmospheres as in an operating fuel cell should suffer the least from the stability problems and is thus the recommended method.

7.7. Recommendation for the uniform practices

Finally we put forward four key recommendations based on our analyses and observations for measuring the oxygen and carbonate ion as well as proton conductivities in (wet) hydrogen, air or O_2 and CO_2 atmospheres. The methods are listed in order of preference, but cases 1 and 2 are only recommended if both mass flows and voltage can be measured accurately, e.g. with the Luggin probe geometry.

1) The product analysis method using the same gases as in a working fuel cell is well suitable for fast measurements. All ionic and electronic conductivities can in principle be measured simultaneously. Also in case of hydrogen, there should not be any extra stability issues when the effect of "extrinsic ions" is measured.
2) In case the electronic and a specific ion conductivity are measured simultaneously, it is recommended to use the product analysis method in which active gas is fed to one side and passive gas to the other side of the sample. In case of hydrogen, it is recommended to first measure the conductivity with dry passive gas and moving to wet passive gas in case of stability issues.
3) If accurate mass flow measurements were not possible, a 4-point constant current method with either bar or Luggin probe geometries is recommended. In case of hydrogen, testing first with dry hydrogen and then moving to wet hydrogen is advisable if there are stability issues.
4) The 2-point constant current measurement is a simple, but slow method as preferably at least 5 different electrolyte thicknesses should be used. In case of hydrogen, it is recommended to first test with dry hydrogen and then moving to wet hydrogen, if stability issues occur.

If for some reason, cases 2 to 4 would not work with wet gases when measuring in hydrogen atmospheres, the case 1 could be used instead. In cases 3 and 4, the level of the electronic conductivity is good to check, e.g. with the Hebb–Wagner method. Finally, when employing the electrolyte in a fuel cell measurement, its thickness and the types of electrodes should clearly be reported as this information is often missing in the reviewed articles.

8. Conclusions

In this paper we have reviewed the ionic conductivity measurement techniques and conductivity values for low temperature solid oxide fuel cell (LT-SOFC) composite electrolytes. One aim was to understand how the different techniques and conditions may affect the conductivity values. Reviewing the literature clearly shows that the electrochemical impedance spectroscopy (EIS) has been the most common method for determining the ionic conductivity of the doped ceria/carbonate composite electrolyte samples. Regrettably, a high or low EIS conductivity value alone does

not necessarily determine how an electrolyte would perform in real fuel cell conditions. The reason for this is that most of the ions that contribute in the EIS to the total conductivity, do not participate to the actual conduction in the real fuel cell conditions. For this reason the conductivities measured with EIS are thus generally higher than in reality. The constant current and product analysis measurements (two other common techniques for determining the conductivity) should therefore give more realistic values for the ionic conductivity during the operation of a fuel cell.

When one measures the ionic conductivity, there are always electrode reactions that can affect the measurement. The contributions from the electrodes have been circumvented using EIS, 4-point and current interruption methods and the 4-point method can be recommended for most of the measurements if the measurement probes are positioned correctly. In some recent articles this was overlooked which could cause a clear error in the conductivity value. The electronic conductivity in the composites needs also more attention in the future as it has not yet been addressed properly. Additionally, it was noted that the preparation methods and materials affect greatly the conductivity properties of the LTSOFC composite electrolytes and should be clearly reported in connection with the measurements.

Based on our analysis, the EIS cannot be recommended to be used when a sample has several different conduction mechanisms. However, the constant current and product analysis methods can give accurate values if conducted correctly. For this reason we have included recommendations for the measurement configuration when using these methods. It would also be a good practice to perform fuel cell measurements along with the conductivity measurements so that the effective goodness of the electrolyte during the fuel cell operation could be estimated.

As a next step in improving the accuracy of the characterization methods of the ionic conductivities of LT-SOFC materials, we recommend a detailed experimental study using the measurement methods mentioned here for a reference sample. Based on such a study, one could then move forward to creating more reliable reference values for the ionic conductivities of new LT-SOFC material sets.

Acknowledgment

The Finnish Funding Agency for Technology and Innovation, TEKES, is acknowledged for their financial support for the article. Dr. Y. Ma acknowledges support through the EU FP7 individual Marie Curie fellowship.

References

[1] F. Jeffrey, H. Rob, L. Xianguo, P.W. David, Z. Jiujun, Solid Oxide Fuel Cells: Materials Properties and Performance, CRC Press, 2009.
[2] R. O'Hayre, Fuel Cell Fundamentals, Wiley, New York, 2006.
[3] C. Xia, Y. Li, Y. Tian, Q. Liu, Z. Wang, L. Jia, Y. Zhao, Y. Li, J. Power Sources 195 (2010) 3149–3154.
[4] L. Fan, C. Wang, M. Chen, B. Zhu, J. Power Sources 234 (2013) 154–174.
[5] S.R. Hui, J. Roller, S. Yick, X. Zhang, C. Decès-Petit, Y. Xie, R. Maric, D. Ghosh, J. Power Sources 172 (2007) 493–502.
[6] X. Wang, Y. Ma, B. Zhu, Int. J. Hydrogen Energy 37 (2012) 19417–19425.
[7] Z. Shao, W. Zhou, Z. Zhu, Prog. Mater. Sci. 57 (2012) 804–874.
[8] J.W. Fergus, J. Power Sources 162 (2006) 30–40.
[9] C. Sun, H. Li, L. Chen, Energy Environ. Sci. 5 (2012) 8475–8505.
[10] V.V. Kharton, F.M.B. Marques, A. Atkinson, Solid State Ionics 174 (2004) 135–149.
[11] L. Zhang, X. Li, S. Wang, K.G. Romito, K. Huang, Electrochem. Commun. 13 (2011) 554–557.
[12] T. Cai, Y. Zeng, S. Yin, L. Wang, C. Li, Mater. Lett. 65 (2011) 2751–2754.
[13] X. Wang, Y. Ma, R. Raza, M. Muhammed, B. Zhu, Electrochem. Commun. 10 (2008) 1617–1620.
[14] R. Chockalingam, S. Basu, Int. J. Hydrogen Energy 36 (2011) 14977–14983.
[15] J. Huang, Z. Gao, Z. Mao, Int. J. Hydrogen Energy 35 (2010) 4270–4275.
[16] M. Benamira, A. Ringuedé, V. Albin, R.N. Vannier, L. Hildebrandt, C. Lagergren, M. Cassir, J. Power Sources 196 (2011) 5546–5554.
[17] V. Jain, S. Bobade, D. Gulwade, P. Gopalan, Ionics 16 (2010) 487–496.
[18] I. Solodkyi, H. Borodianska, Y. Sakka, O. Vasylkiv, J. Nanosci. Nanotechnol. 12 (2012) 1871–1879.
[19] J. Wu, B. Zhu, Y. Mi, S.-J. Shih, J. Wei, Y. Huang, J. Power Sources 201 (2012) 164–168.
[20] Z. Gao, R. Raza, B. Zhu, Z. Mao, C. Wang, Z. Liu, Int. J. Hydrogen Energy 36 (2011) 3984–3988.
[21] C. Xia, Y. Li, Y. Tian, Q. Liu, Y. Zhao, L. Jia, Y. Li, J. Power Sources 188 (2009) 156–162.
[22] A.S.V. Ferreira, C.M.C. Soares, F.M.H.L.R. Figueiredo, F.M.B. Marques, Int. J. Hydrogen Energy 36 (2011) 3704–3711.
[23] B.C.H. Steele, Solid State Ionics 129 (2000) 95–110.
[24] A. Radojkovic, M. Žunic, S.M. Savic, G. Brankovic, Z. Brankovic, Ceram. Int. 39 (2013) 307–313.
[25] H.L. Tuller, Solid State Ionics 131 (2000) 143–157.
[26] Y. Ma, X. Wang, R. Raza, M. Muhammed, B. Zhu, Int. J. Hydrogen Energy 35 (2010) 2580–2585.
[27] J. Huang, L. Yang, R. Gao, Z. Mao, C. Wang, Electrochem. Commun. 8 (2006) 785–789.
[28] L. Zhang, R. Lan, A. Kraft, S. Tao, Electrochem. Commun. 13 (2011) 582–585.
[29] L. Zhang, R. Lan, C.T.G. Petit, S. Tao, Int. J. Hydrogen Energy 35 (2010) 6934–6940.
[30] S. Li, J. Sun, Int. J. Hydrogen Energy 35 (2010) 2980–2985.
[31] B. Zhu, R. Raza, Q. Liu, H. Qin, Z. Zhu, L. Fan, M. Singh, P. Lund, RSC Adv. 2 (2012) 5066–5070.
[32] Q. Liu, H. Qin, R. Raza, L. Fan, Y. Li, B. Zhu, RSC Adv. 2 (2012) 8036–8040.
[33] H. Qin, B. Zhu, R. Raza, M. Singh, L. Fan, P. Lund, Int. J. Hydrogen Energy 37 (2012) 19365–19370.
[34] L. Fan, C. Wang, O. Osamudiamen, R. Raza, M. Singh, B. Zhu, J. Power Sources 217 (2012) 164–169.
[35] H.P. He, X.J. Huang, L.Q. Chen, Ionics 6 (2000) 64–69.
[36] Y. Xia, X. Liu, Y. Bai, H. Li, X. Deng, X. Niu, X. Wu, D. Zhou, M. Lv, Z. Wang, J. Meng, RSC Adv. 2 (2012) 3828–3834.
[37] B. Zhu, L. Fan, P. Lund, Appl. Energy 106 (2013) 163–175.
[38] S.C. Singhal, K. Kendall, High-Temperature Solid Oxide Fuel Cells: Fundamentals, Design and Applications, Elsevier, Oxford, 2003.
[39] J. Di, M. Chen, C. Wang, J. Zheng, L. Fan, B. Zhu, J. Power Sources 195 (2010) 4695–4699.
[40] Z. Bin, Solid State Ionics 145 (2001) 371–380.
[41] D. Pérez-Coll, A. Aguadero, P. Núñez, J.R. Frade, Int. J. Hydrogen Energy 35 (2010) 11448–11455.
[42] D.P. Sutija, T. Norby, P. Björnbom, Solid State Ionics 77 (1995) 167–174.
[43] H.K. Bentzer, N. Bonanos, J.W. Phair, Solid State Ionics 181 (2010) 249–255.
[44] J.R. Macdonald, Impedance Spectroscopy: Emphasizing Solid Materials and Systems, Wiley, 1987.
[45] A.J. Bard, L.R. Faulkner, Electrochemical Methods: Fundamentals and Applications, second ed., Wiley, New York (N.Y.), 2001.
[46] I. Kosacki, B. Gorman, H.U. Anderson, T.A. Ramanarayanan, W.L. Worrell, H.L. Tuller, A.C. Khandkar, M. Mogensen, W. Gopel, Electrochem. Soc. III (1998) 631.
[47] A. Bodén, J. Di, C. Lagergren, G. Lindbergh, C.Y. Wang, J. Power Sources 172 (2007) 520–529.
[48] J. Huang, Z. Mao, Z. Liu, C. Wang, Electrochem. Commun. 9 (2007) 2601–2605.
[49] R. Raza, X. Wang, Y. Ma, B. Zhu, J. Power Sources 195 (2010) 6491–6495.
[50] J. Huang, F. Xie, C. Wang, Z. Mao, Int. J. Hydrogen Energy 37 (2012) 877–883.
[51] X. Li, G. Xiao, K. Huang, J. Electrochem. Soc. 158 (2011) B225–B232.
[52] M. Benamira, A. Ringuedé, L. Hildebrandt, C. Lagergren, R.N. Vannier, M. Cassir, Int. J. Hydrogen Energy 37 (2012) 19371–19379.
[53] L. Fan, C. Wang, J. Di, M. Chen, J. Zheng, B. Zhu, J. Nanosci. Nanotechnol. 12 (2012) 4941–4945.
[54] C.M. Lapa, F.M.L. Figueiredo, D.P.F. de Souza, L. Song, B. Zhu, F.M.B. Marques, Int. J. Hydrogen Energy 35 (2010) 2953–2957.
[55] Z. Tang, Q. Lin, B.-E. Mellander, B. Zhu, Int. J. Hydrogen Energy 35 (2010) 2970–2975.
[56] A.S.V. Ferreira, T. Saradha, F.L. Figueiredo, F.M.B. Marques, Int. J. Energy Res. 35 (2011) 1090–1099.
[57] T. Saradha, A.S. Fereira, S.G. Patrício, F.M.L. Figueiredo, F.M.B. Marques, Int. J. Hydrogen Energy 37 (2012) 7235–7241.
[58] Y. Ma, X. Wang, H.A. Khalifa, B. Zhu, M. Muhammed, Int. J. Hydrogen Energy 37 (2012) 19401–19406.
[59] G. Hsieh, T.O. Mason, E.J. Garboczi, L.R. Pederson, Solid State Ionics 96 (1997) 153–172.
[60] G. Abbas, R. Raza, M.A. Chaudhry, B. Zhu, J. Fuel Cell. Sci. Technol. 8 (2011) 041013.
[61] R. Raza, H. Qin, L. Fan, K. Takeda, M. Mizuhata, B. Zhu, J. Power Sources 201 (2012) 121–127.
[62] N. Zuo, M. Zhang, Z. Mao, Z. Gao, F. Xie, J. Eur. Ceram. Soc. 31 (2011) 3103–3107.
[63] Y. Xia, Y. Bai, X. Wu, D. Zhou, X. Liu, J. Meng, Int. J. Hydrogen Energy 36 (2011) 6840–6850.
[64] Z. Gao, J. Huang, Z. Mao, C. Wang, Z. Liu, Int. J. Hydrogen Energy 35 (2010) 731–737.
[65] P. Patnaik, Handbook of Inorganic Chemical Compounds, McGraw-Hill, 2003.

[66] W. Zhu, C. Xia, D. Ding, X. Shi, G. Meng, Mater. Res. Bull. 41 (2006) 2057–2064.
[67] J. Di, M.M. Chen, C.Y. Wang, J.M. Zheng, B. Zhu, Adv. Mater. Res. 105–106 (2010) 687–690.
[68] M. Joachim, Prog. Solid State Chem. 23 (1995) 171–263.
[69] E.J. Zimney, G.H.B. Dommett, D.R.S. Ruoff, Meas. Sci. Technol. 18 (2007) 2067.
[70] Z. Xie, C. Song, B. Andreaus, T. Navessin, Z. Shi, J. Zhang, S. Holdcroft, J. Electrochem. Soc. 153 (2006) E173–E178.
[71] L. Fan, G. Zhang, M. Chen, C. Wang, J. Di, B. Zhu, Int. J. Electrochem. Sci. 7 (2012) 8420–8435.
[72] X. Wang, Y. Ma, S. Li, A.-H. Kashyout, B. Zhu, M. Muhammed, J. Power Sources 196 (2011) 2754–2758.
[73] X. Wang, Y. Ma, S. Li, B. Zhu, M. Muhammed, Int. J. Hydrogen Energy 37 (2012) 19380–19387.
[74] Y. Zhao, Z. Xu, C. Xia, Y. Li, Int. J. Hydrogen Energy 38 (2013) 1553–1559.
[75] W. Liu, Y. Liu, B. Li, T.D. Sparks, X. Wei, W. Pan, Compos. Sci. Technol. 70 (2010) 181–185.
[76] I. Riess, in: T.A. Ramanarayanan, W.L. Worrell, H.L. Tuller (Eds.), Ionic and Mixed Conducting Ceramics, vol. 94-12, The Electrochemical Society, Pennington, NJ, 1994, pp. 286–306.
[77] I. Riess, Solid State Ionics 91 (1996) 221–232.
[78] Y. Zhao, C. Xia, Y. Wang, Z. Xu, Y. Li, Int. J. Hydrogen Energy 37 (2012a) 8556–8561.
[79] Y. Zhao, C. Xia, Z. Xu, Y. Li, Int. J. Hydrogen Energy 37 (2012b) 11378–11382.
[80] F. Barbir, PEM Fuel Cells: Theory and Practice, Elsevier Academic Press, 2005.
[81] K.R. Cooper, M. Smith, J. Power Sources 160 (2006) 1088–1095.
[82] M.J. Deen, F. Pascal, J. Mater. Sci. Mater. Electron. 17 (2006) 549–575.
[83] G.J. Janz, M.R. Lorenz, J. Chem. Eng. Data 6 (1961) 321–323.
[84] R. Chockalingam, S. Jain, S. Basu, Integr. Ferroelectr. 116 (2010) 23–34.
[85] Z. Gao, R. Raza, B. Zhu, Z. Mao, J. Nanosci. Nanotechnol. 11 (2011) 5413–5417.
[86] L. Fan, C. Wang, M. Chen, J. Di, J. Zheng, B. Zhu, Int. J. Hydrogen Energy 36 (2011) 9987–9993.
[87] T. Ristoiu, T. P Jr., M. Gabor, S. Rada, F. Popa, L. Ciontea, T. Petrisor, J. Alloys Compd. 532 (2012) 109–113.
[88] X. Wang, Dual-ion Conducting Nanocomposite for Low Temperature Solid Oxide Fuel Cell (Ph.D. thesis), KTH, Functional Materials, FNM, 2012. QC 20120529.